N78-70090

Accession No. 54059-64

Copy No. SID 63-1520

HIGH-VACUUM PLUME IMPINGEMENT TEST REPORT

25 February 1964

Exhibit I, Paragraph 5.5

(NASA-CR-155264) HIGH VACUUM PLUME IMPINGEMENT TEST REPORT (North American Aviation, Inc.) 67 p

N78-70090

Unclas

00/20 33768

REPRODUCED BY
NATIONAL TECHNICAL
INFORMATION SERVICE
U.S. DEPARTMENT OF COMMERCE
SPRINGFIELD, VA. 22161

NORTH AMERICAN AVIATION, INC.
SPACE and INFORMATION SYSTEMS DIVISION

64

FOREWORD

The Apollo Jet Plume Tests were conducted under NASA Apollo Contract NAS 9-150.

This report was prepared by E. T. Piesik and M. L. Lofland of the Propulsion Analysis Section of Apollo Engineering, Space and Information Systems Division, North American Aviation, Inc.

Preceding page blank

ABSTRACT

The thermal protection design required to shield the Apollo service module skin from the reaction control system engine exhaust impingement has been determined from the test program data described in this report.

The simulated space engine exhaust impingement tests with a prototype Apollo service module reaction control system engine (SM RCS) and a flat surface were conducted in J2A test cell of the Rocket Test Facility at the Arnold Engineering Development Center from 25 March to 28 May 1963. The test conditions simulated pressure altitudes between 400, 000 and 200, 000 feet.

Surface heating rate and pressure distribution data are given for the flat-plate centerline and for one cross section at various engine stand-off distances and nozzle area ratios. In addition, complete heating rate distribution data is presented for the Apollo SM RCS pitch engine design case. The rocket engine, test panel, test cell, and operating conditions are described.

Qualitative information is presented on the effect of surface contamination and visual glare due to the Apollo SM RCS space plume.

Additional reports will be issued at a later date concerning the following items:

1. Heating rate and pressure distribution for a flat plate at various nozzle centerline-to-plate cant angles
2. Theoretical correlation of the data presented
3. The effect of the exhaust boundary area on the heating rate and surface pressure
4. Data on the radiant heating rate exchange between the SM RCS engine and the SM surface.

Preceding page blank

CONTENTS

Section Page

INTRODUCTION 1

I HARDWARE DESCRIPTION 3
  Flat Plate and Actuation System 3
  Thrust Chamber 3

II INSTRUMENTATION 9
  Pressure Measurement, Flat Plate 9
  Heat Transfer Measurement, Flat Plate 9
  Surface Coating Instrumentation, Flat Plate . . . 14
  J2A Test Cell Pressure 14
  Rocket Engine Instrumentation 14
  Photographic Instrumentation 16

III OPERATING CONDITIONS 17
  Test Cell 17
  Rocket Engine 18

IV TEST PROGRAM 21
  Test Criteria 21
  Test Conditions 21
  Heating Rate Data Reduction 27
  Data Reduction and Data Accuracy 31
  Test Results 39

V CONCLUSIONS 61

REFERENCES 63

Preceding page blank

ILLUSTRATIONS

Figure		Page
1	Impingement Panel - Front Surface	4
2	Impingement Panel - Back Side	5
3	Installation of Test Hardware in J2A Test Cell	6
4	SM RCS Rocket Engine with $\epsilon = 40:1$ Molybdenum Nozzle	7
5	SM RCS Nozzle Contour	8
6	Pressure Transducer Locations	10
7	Pressure Transducer Locations, $\epsilon = 10:1$	11
8	Thermocouple Installation	12
9	Thermocouple Locations	13
10	Detail of Radiator Coating Specimen and Holder	15
11	AEDC J2A Test Cell	19
12	Coordinate System	26
13	Ambient Pressure - Time Variation of the J2A Test Cell	28
14	Plume Boundary Profiles on Impingement Panel	29
15	Specific Heat Versus Temperature for 18-8 Stainless Steel	30
16	Temperature - Time Histories $\epsilon = 10:1$ (Thermocouples undisturbed by boundary region)	32
17	Temperature - Time Histories $\epsilon = 15:1$ (Thermocouples undisturbed by boundary region)	33
18	Temperature - Time Histories $\epsilon = 20:1$ (Thermocouples undisturbed by boundary region)	34
19	Temperature - Time Histories $\epsilon = 40:1$ (Thermocouples undisturbed by boundary region)	35
20	Temperature - Time Histories $\epsilon = 40:1$ (Thermocouples influenced by boundary region)	36
21	Temperature - Time Histories $\epsilon = 40:1$ (Typical data repeatability)	37
22	Surface Pressure - Time Histories $\epsilon = 10:1$	38
23	Heating Rate Distribution $\epsilon = 10:1$	40
24	Heating Rate Distribution $\epsilon = 10:1$	41
25	Heating Rate Distribution $\epsilon = 10:1$	42
26	Heating Rate Distribution $\epsilon = 15:1$	43
27	Heating Rate Distribution $\epsilon = 15:1$	44
28	Heating Rate Distribution $\epsilon = 20:1$	45

Preceding page blank

Figure Page

29 Heating Rate Distribution $\epsilon = 20:1$ 46
30 Heating Rate Distribution, Apollo SM RCS Design Case, $\epsilon = 40:1$ 47
31 Heating Rate Distribution, Apollo SM RCS Design Case, $\epsilon = 40:1$ 48
32 Heating Rate Distribution, Apollo SM RCS Design Case, $\epsilon = 40:1$ 49
33 Heating Rate Distribution, Apollo SM RCS Design Case, $\epsilon = 40:1$ 50
34 Heating Rate Distribution, Apollo SM RCS Design Case, $\epsilon = 40:1$ 51
35 Heating Rate Map, Apollo SM RCS Design Case, $\epsilon = 40:1$ 52
36 Surface Pressure Distribution, $\epsilon = 10:1$ 54
37 Surface Pressure Distribution, $\epsilon = 10:1$ 55
38 Surface Pressure Distribution, $\epsilon = 10:1$ 56
39 Comparison of Centerline Heating Rate and Pressure Distributions, $\epsilon = 10:1$ 57
40 Exhaust Flow Field Visualization $\epsilon = 40:1$ 58
41 Exhaust Flow Field Visualization $\epsilon = 15:1$ 59

TABLES

Table Page

1 Test Run Schedule 22

INTRODUCTION

In a space environment, the exhaust of a rocket engine may expand so as to impinge upon the spacecraft structure or its components. This exhaust gas impingement will result in surface heating, pressure, and perhaps contamination. In order to obtain definition of the problem of exhaust gas impingement on the Apollo service module surface downstream of the reaction control system rocket engine, a full scale test with the Apollo service module reaction control system rocket engine was conducted at Arnold Engineering Development Center RTF J2A test cell. The pressure altitude for this program varied from 400, 000 feet to 200, 000 feet during each rocket engine firing. Additional information concerning this test is presented in the pre-test report, reference 1.

The primary objective of the test was to investigate the heating rate and pressure effects of a simulated space SM RCS exhaust plume impinging on a flat plate. The second objective was to obtain exhaust flow field visualization to assist in data interpretation, and the third objective was to determine the exhaust impingement effects on life and emissivity of radiator surface samples.

Flat-plate heat transfer rate and pressure data were obtained at nozzle-axis-to-plate distances of 3 to 15 nozzle exit radii with cant angles of 0 to 35 degrees. SM RCS engines with nozzle area ratios of 40:1, 20:1, 15:1, and 10:1 were used. This parametric study was performed so that design criteria could be established for the position of the SM RCS engine and the configuration of the heat shield protecting the SM surface.

The problem of thermal protection of the Apollo SM skin from the SM RCS engine exhaust impingement has been solved by the design of a light-weight stainless steel heat shield based on the data presented in this report.

Additional reports will be issued at a later date concerning the following items:

1. Heating rate and pressure distributions for a flat plate at various nozzle centerline to plate cant angles
2. Theoretical correlation of the data presented
3. The effect of the exhaust boundary area on the heating rate and surface pressure
4. Data on the radiant heating rate exchange between the SM RCS engine and the SM surface.

I. HARDWARE DESCRIPTION

FLAT PLATE AND ACTUATION SYSTEM

The instrumented impingement panel, designed and fabricated by NAA, consisted of 18-8 stainless steel sheet, 0.008 inches thick, bonded to a flat section of aluminum honeycomb sandwich 72-inches by 72-inches by 1.0-inch, for structural rigidity. Figure 1 shows the front surface (gas side) of the impingement panel and Figure 2 shows the back (vacuum side) of the panel.

The impingement panel support structure was designed and fabricated by ARO Inc., at AEDC. This structure provided two degrees of freedom (vertical and angular) for remote adjustment of plate stand-off distance and cant angle relative to the rocket engine. Figure 3 shows the panel installation in the J2A test cell.

THRUST CHAMBER

The rocket engine was designed and fabricated by the Marquardt Corporation and reflects the current prototype SM RCS engine design. Four nozzle configurations were tested, one of molybdenum (area ratio 40:1) and three of stainless steel (area ratios 20:1, 15:1, and 10:1). The stainless steel nozzles were fabricated by truncating the basic 40:1 nozzle contour. The propellants used were Aerozine 50 (50 percent UDMH, 50 percent N_2H_4) and nitrogen tetroxide (N_2O_4).

The molybdenum engine with a 40:1 nozzle area ratio is shown in Figure 4, and the nozzle contour is shown in Figure 5.

Preceding page blank

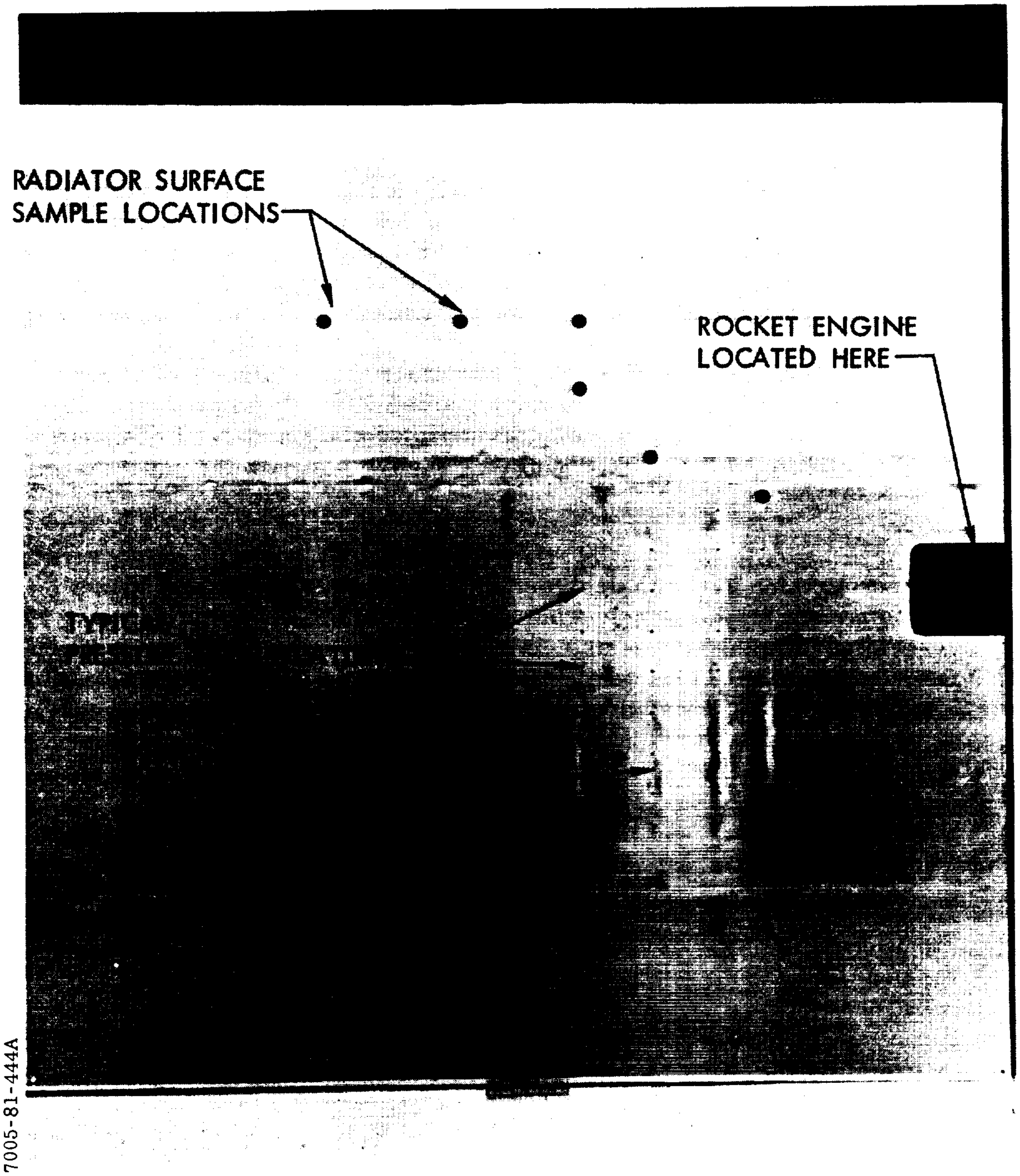
RADIATOR SURFACE
SAMPLE LOCATIONS
ROCKET ENGINE
LOCATED HERE
7005-81-444A

Figure 1. Impingement Panel - Front Surface

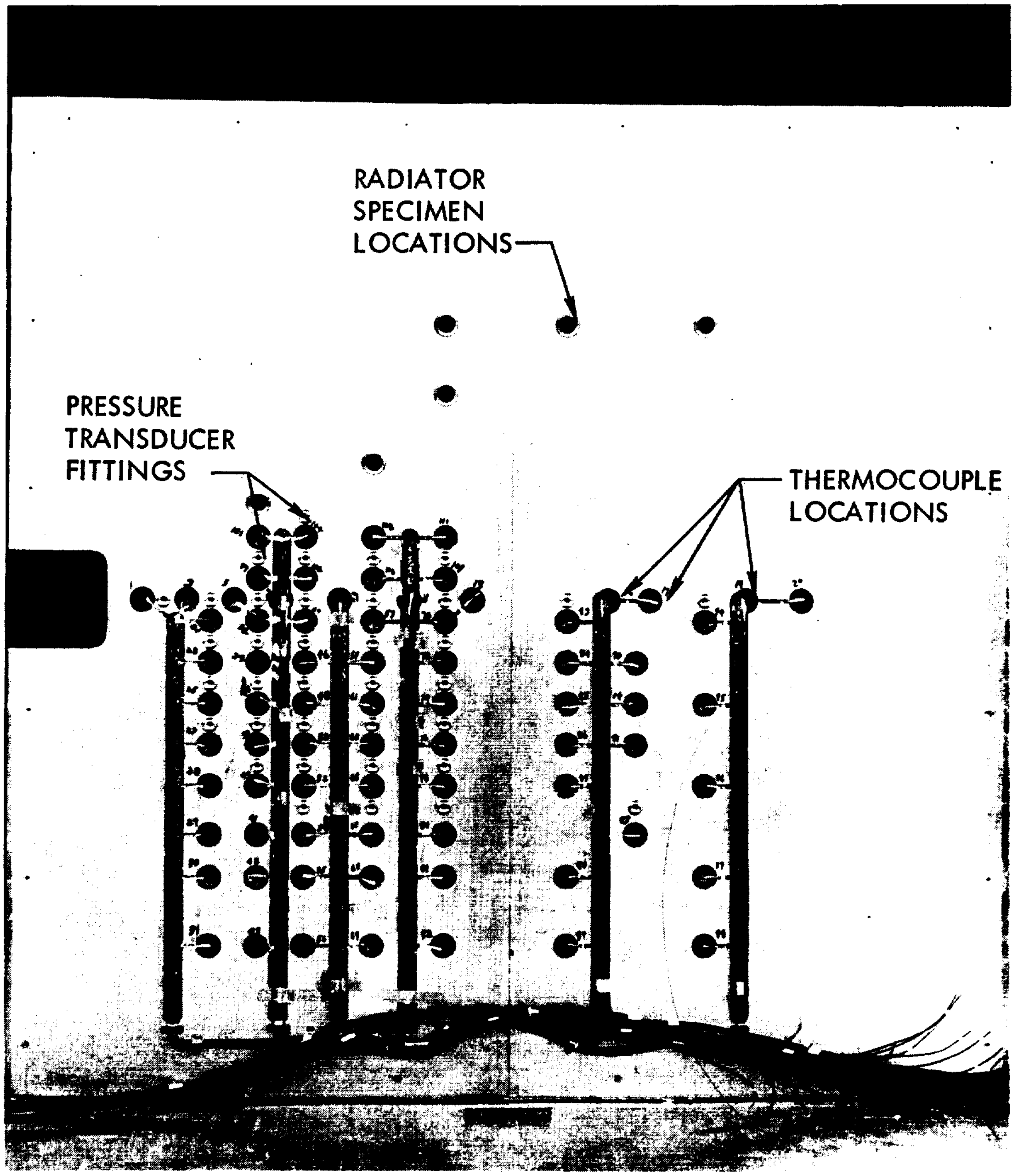
RADIATOR SPECIMEN LOCATIONS
PRESSURE TRANSDUCER FITTINGS
THERMOCOUPLE LOCATIONS
7005-81-444B

Figure 2. Impingement Panel - Back Side

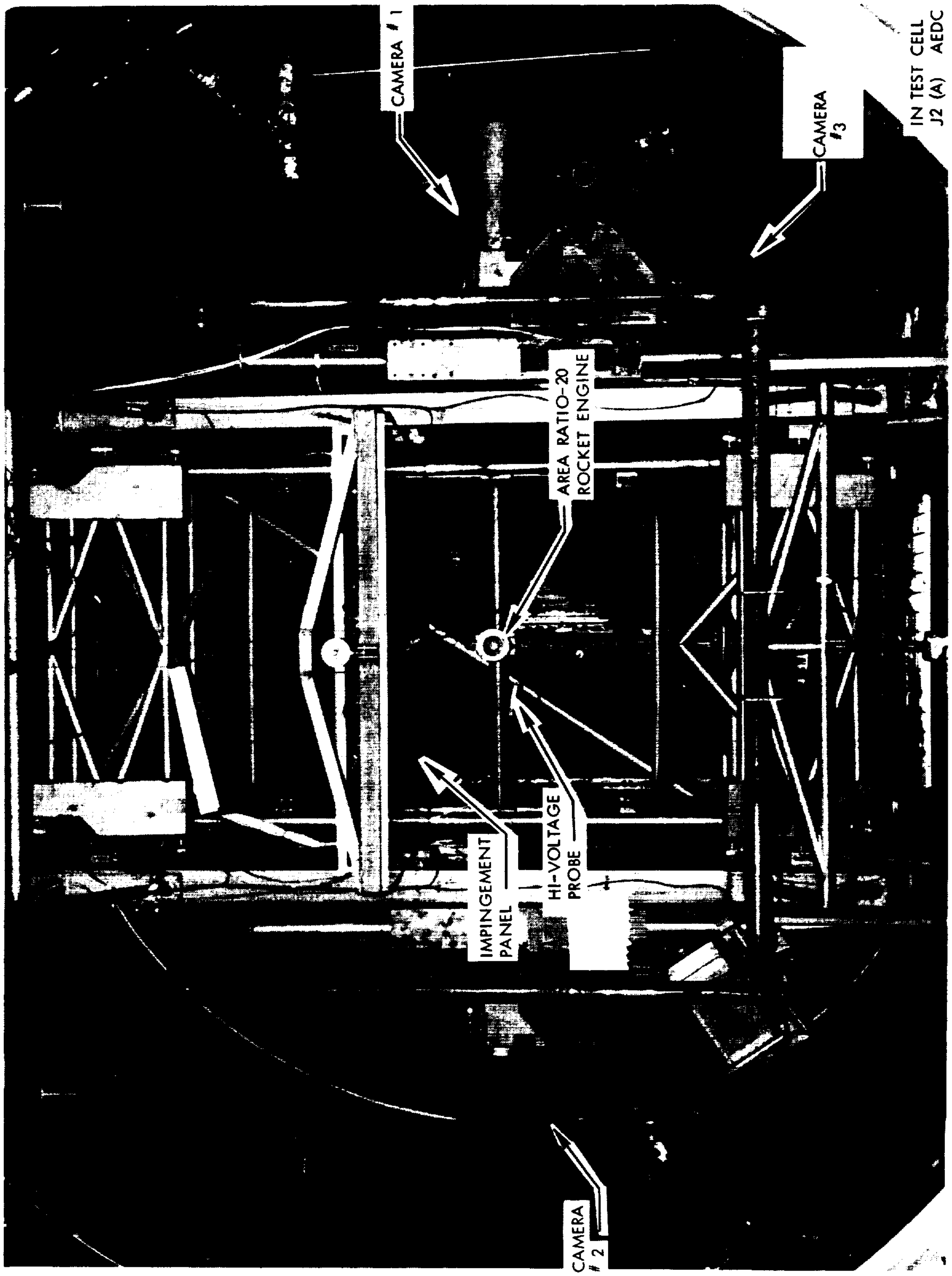
IN TEST CELL J2 (A) AEDC
CAMERA # 1
CAMERA #3
AREA RATIO-20 ROCKET ENGINE
IMPINGEMENT PANEL
HI-VOLTAGE PROBE
CAMERA # 2

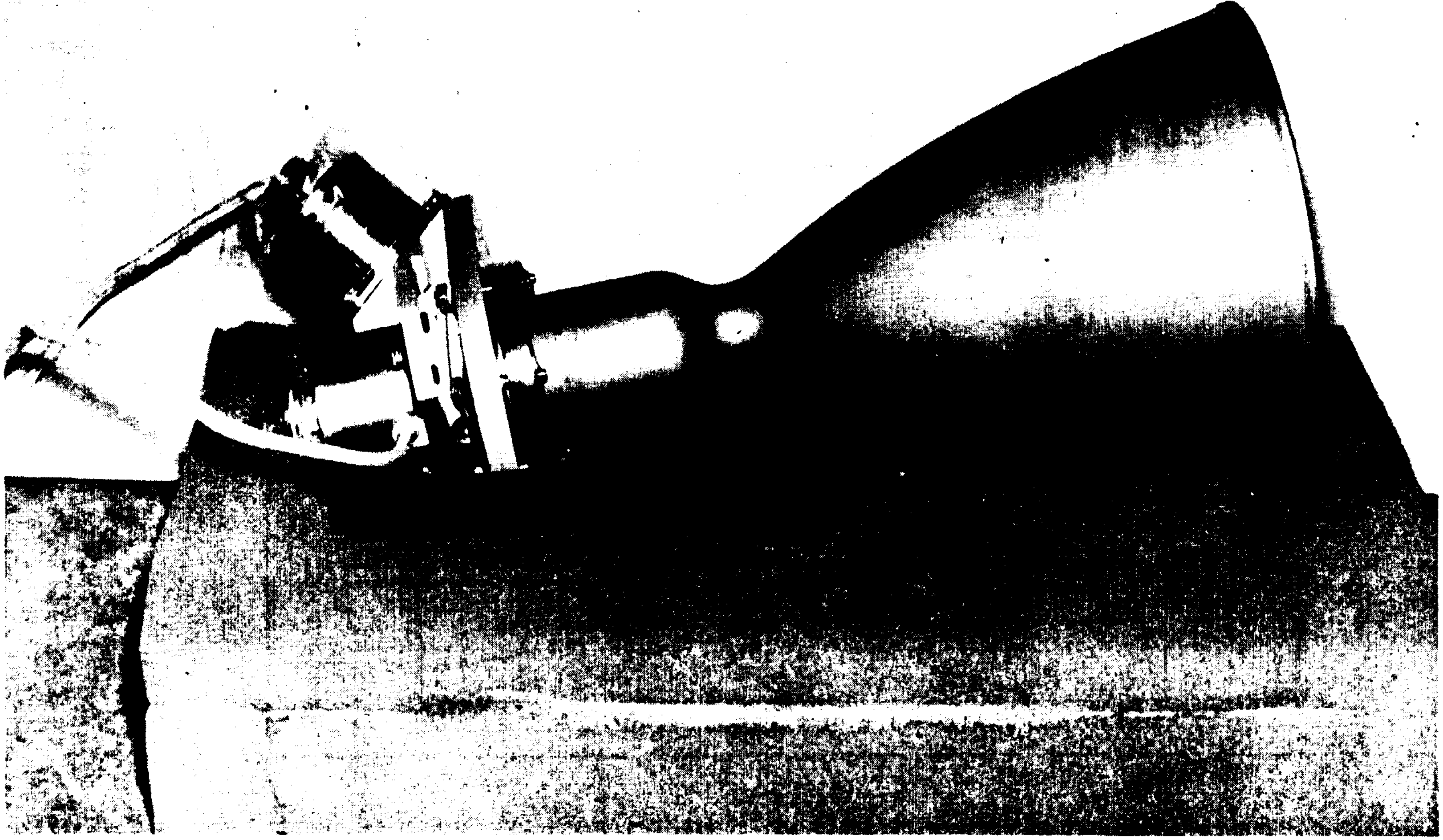

Figure 4. SM RCS Engine With ϵ = 40:1 Molybdenum Nozzle

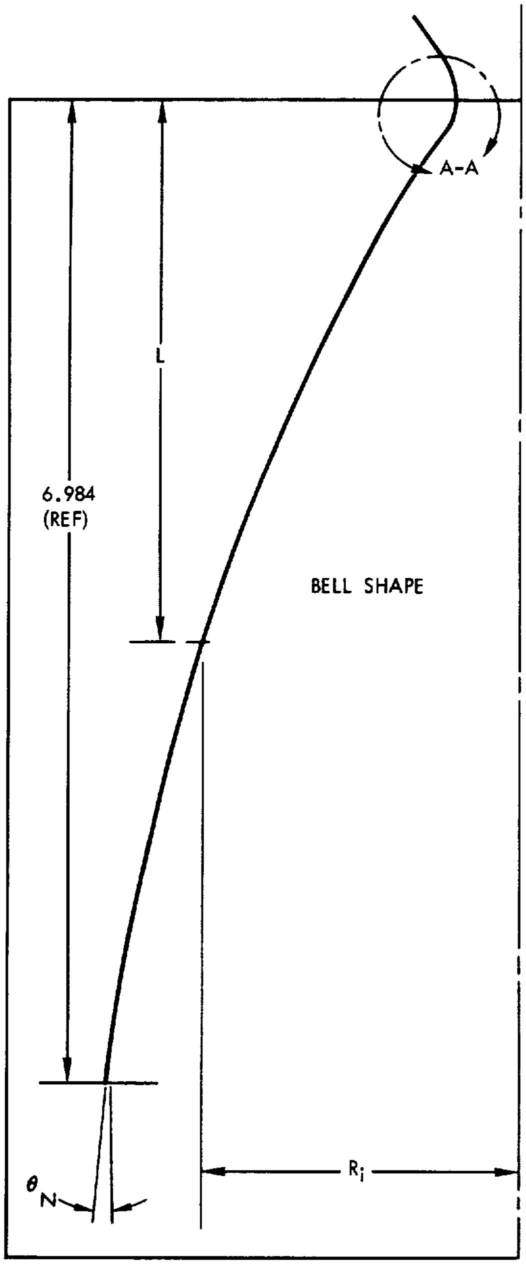
A-A
L
6.984
(REF)
BELL SHAPE
θ_N
R_i

NOZZLE DIMENSIONS

ϵ	40	20	15	10
R_e	2.730	1.941	1.681	1.372
L	6.984	3.447	2.707	1.922
θ_N	8.3°	17°	19°	22°

NOZZLE COORDINATES

L	Ri
0.000	0.434
0.278	0.513
0.474	0.635
0.812	0.832
1.339	1.106
1.866	1.349
2.393	1.565
2.920	1.762
3.447	1.939
3.974	2.101
4.501	2.245
5.028	2.372
5.555	2.483
6.082	2.583
6.609	2.671
6.984	2.730

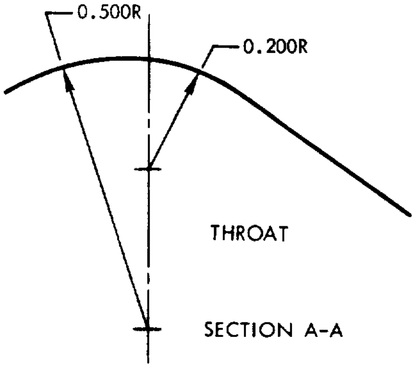
0.500R
0.200R
THROAT
SECTION A-A

Figure 5. SM RCS Nozzle Contour

II. INSTRUMENTATION

PRESSURE MEASUREMENT, FLAT PLATE

Thirty-six pressure transducers were located as shown in Figure 6 and attached to the backside of the panel where threaded blocks were provided. Pressure transducers having two ranges (0-0.1 psid and 0-1.0 psia) were arranged alternately to allow complete surface and range coverage for one side of the panel centerline. The five transducers placed on the other side were used to spot check the symmetry of flow. During the area ratio 10:1 runs, the pressure transducers were rearranged slightly (see Figure 7) to obtain better range coverage for the expected higher surface pressures. The differential-type gages were referenced to the cell pressure. The pressure transducers (Models PT 14-01 and APT 85-1) were manufactured by Dynisco. The strain gage type of pressure transducer was chosen because of the incompatibility of J2A test cell with any other type of pressure instrumentation, and the low level of confidence that any type of pressure transducer would be effective at the expected pressure range and in the environment of J2A test cell.

Controlled heating bars were installed in the proximity of the transducers to maintain the temperature near 70 F. Thermocouples placed on the transducers were monitored during the test.

HEAT TRANSFER MEASUREMENT, FLAT PLATE

Heat rates due to exhaust gas impingement on the flat plate were obtained by the "thin skin" method. An effort was made to reduce to a negligible amount the heat loss from the measurement point. Seventy-five thermocouples were spotwelded, to ensure good thermal contact to the back side of the 0.008-inch stainless steel sheet, through 1.75-inch diameter relief holes provided in the honeycomb panel (Figure 8). Thus the tangential conduction path in the thin skin to the honeycomb structure was 0.78 inch. To reduce conduction along the thermocouple leads, the thermocouples consisted of 36-gage chromel-alumel wire approximately 2 inches in length, joined with 18-gage copper-constantan extension wire. The 36-gage wires were individually welded to the thin skin with a 3/16 inch gap between the junctions. This gap reduced the error due to the change in skin thickness at the weld, since the temperature measured was that of the metal between the junctions of the thermocouple. The thermocouple locations are shown in Figure 9.

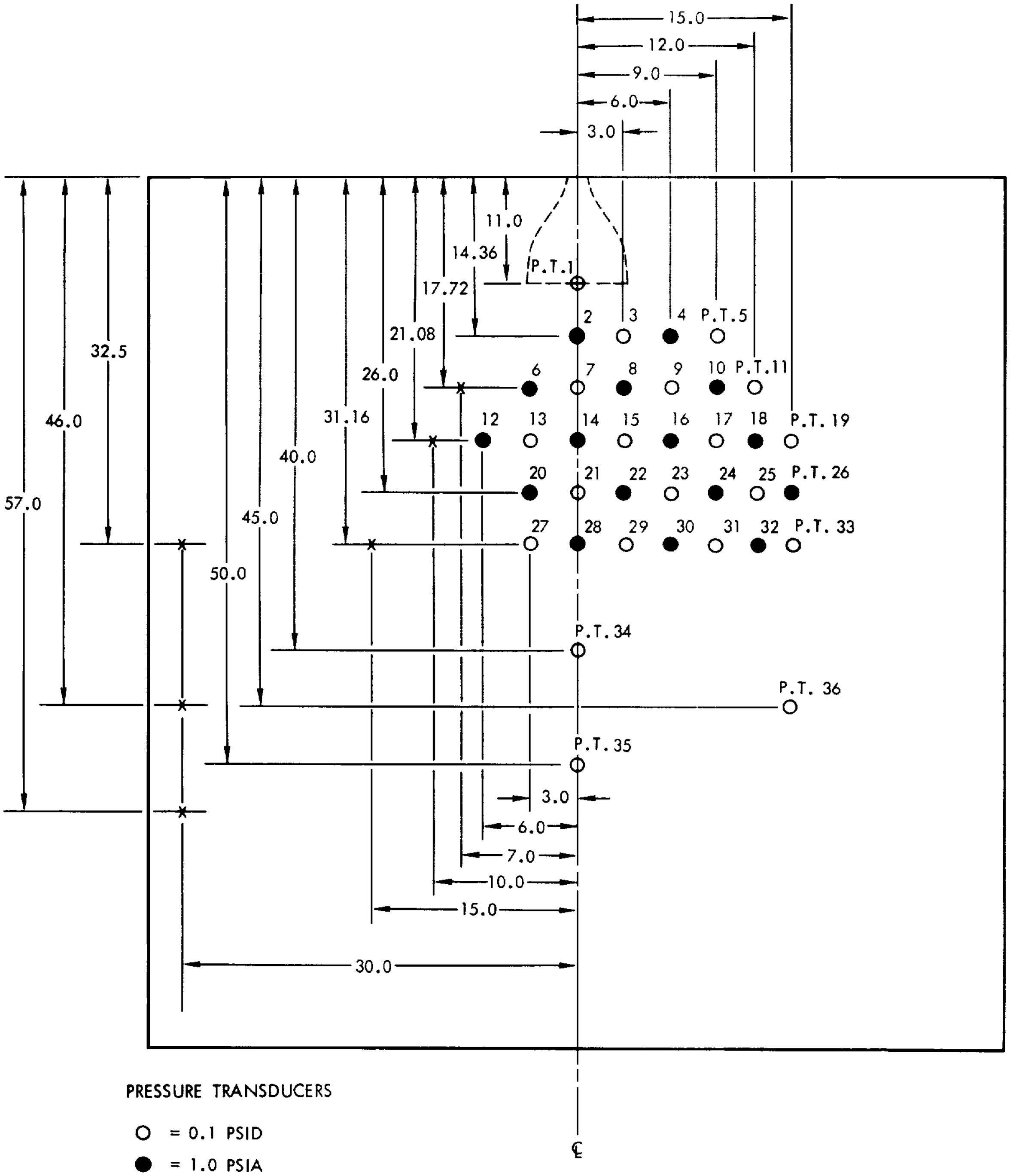
15.0
12.0
9.0
6.0
3.0
11.0
14.36
17.72
21.08
26.0
31.16
32.5
46.0
57.0
40.0
45.0
50.0
P.T.1
2
3
4
P.T.5
6
7
8
9
10
P.T.11
12
13
14
15
16
17
18
P.T. 19
20
21
22
23
24
25
P.T. 26
27
28
29
30
31
32
P.T. 33
P.T. 34
P.T. 36
P.T. 35
3.0
6.0
7.0
10.0
15.0
30.0
℄

PRESSURE TRANSDUCERS

○ = 0.1 PSID

● = 1.0 PSIA

X RADIATOR SURFACE SPECIMENS

NOTE:

1. ALL DIMENSIONS ARE GIVEN IN INCHES.
2. THIS IS A VIEW OF THE FRONT SIDE OF THE IMPINGEMENT PANEL.

Figure 6. Pressure Transducer Locations

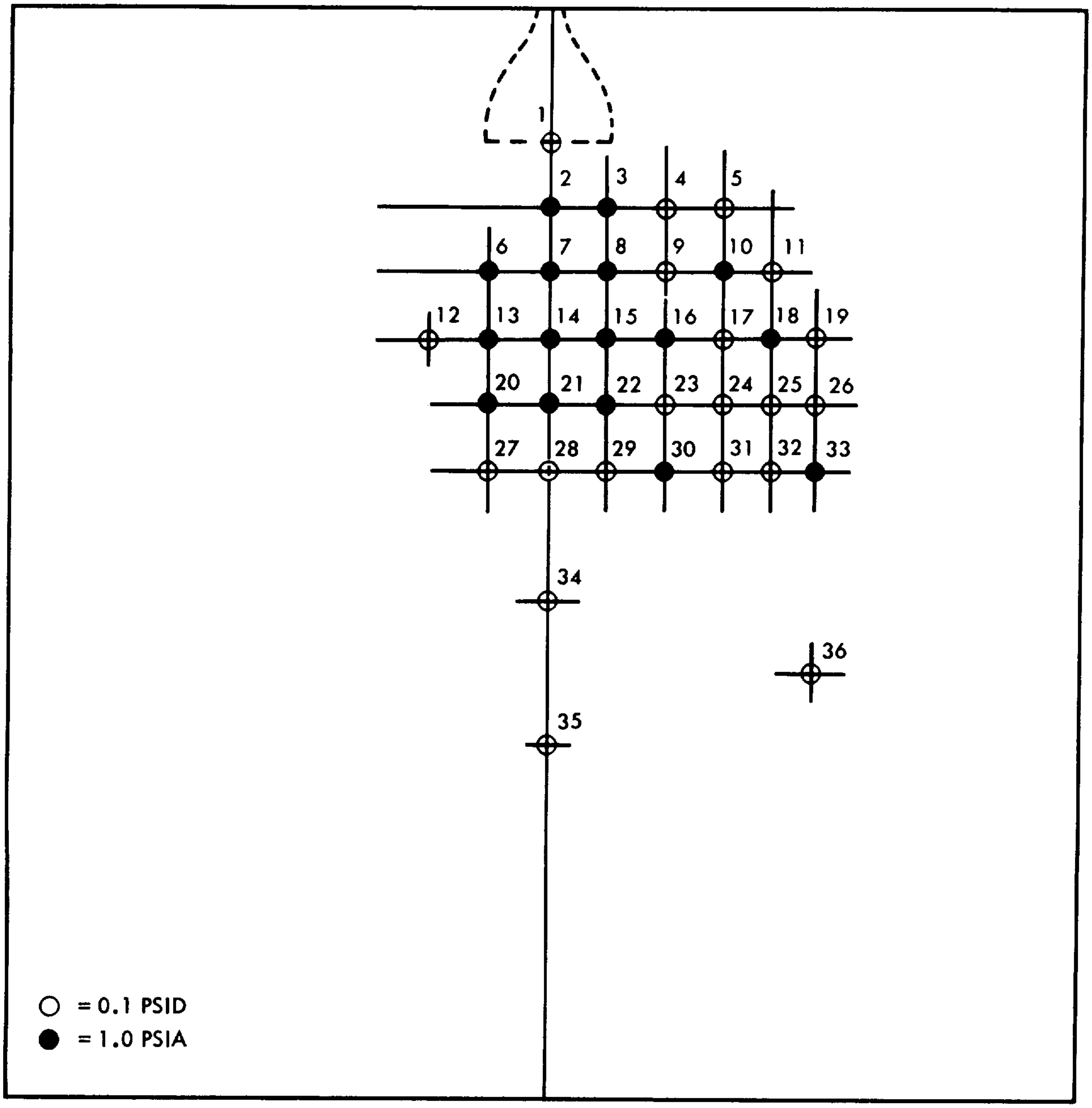
1
2
3
4
5
6
7
8
9
10
11
12
13
14
15
16
17
18
19
20
21
22
23
24
25
26
27
28
29
30
31
32
33
34
35
36
○ = 0.1 PSID
● = 1.0 PSIA

Figure 7. Pressure Transducer Locations, ϵ = 10:1

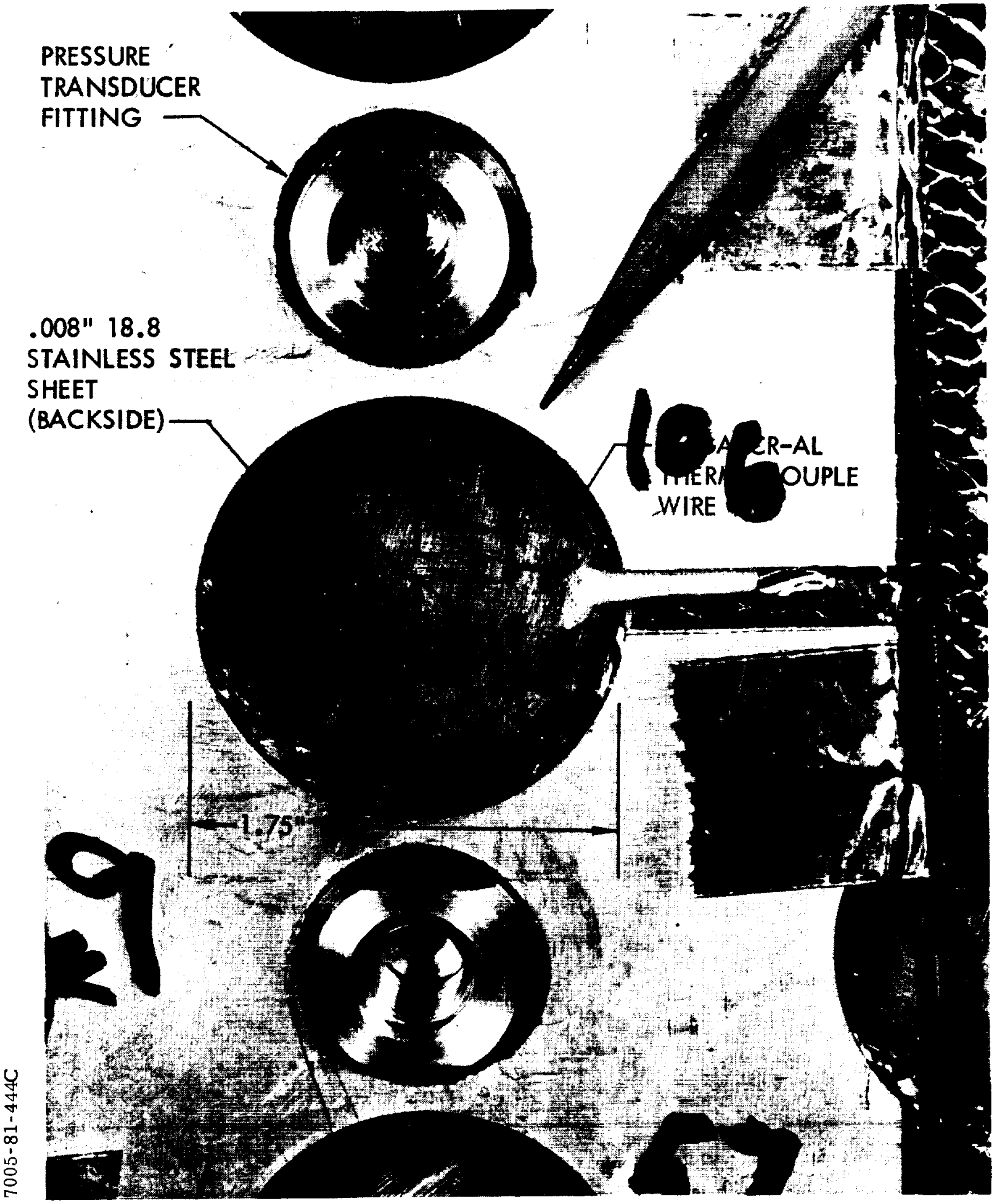
PRESSURE TRANSDUCER FITTING
.008" 18.8 STAINLESS STEEL SHEET (BACKSIDE)
R-AL THERMOCOUPLE WIRE
10
6
1.75"
9
7005-81-444C

Figure 8. Thermocouple Installation

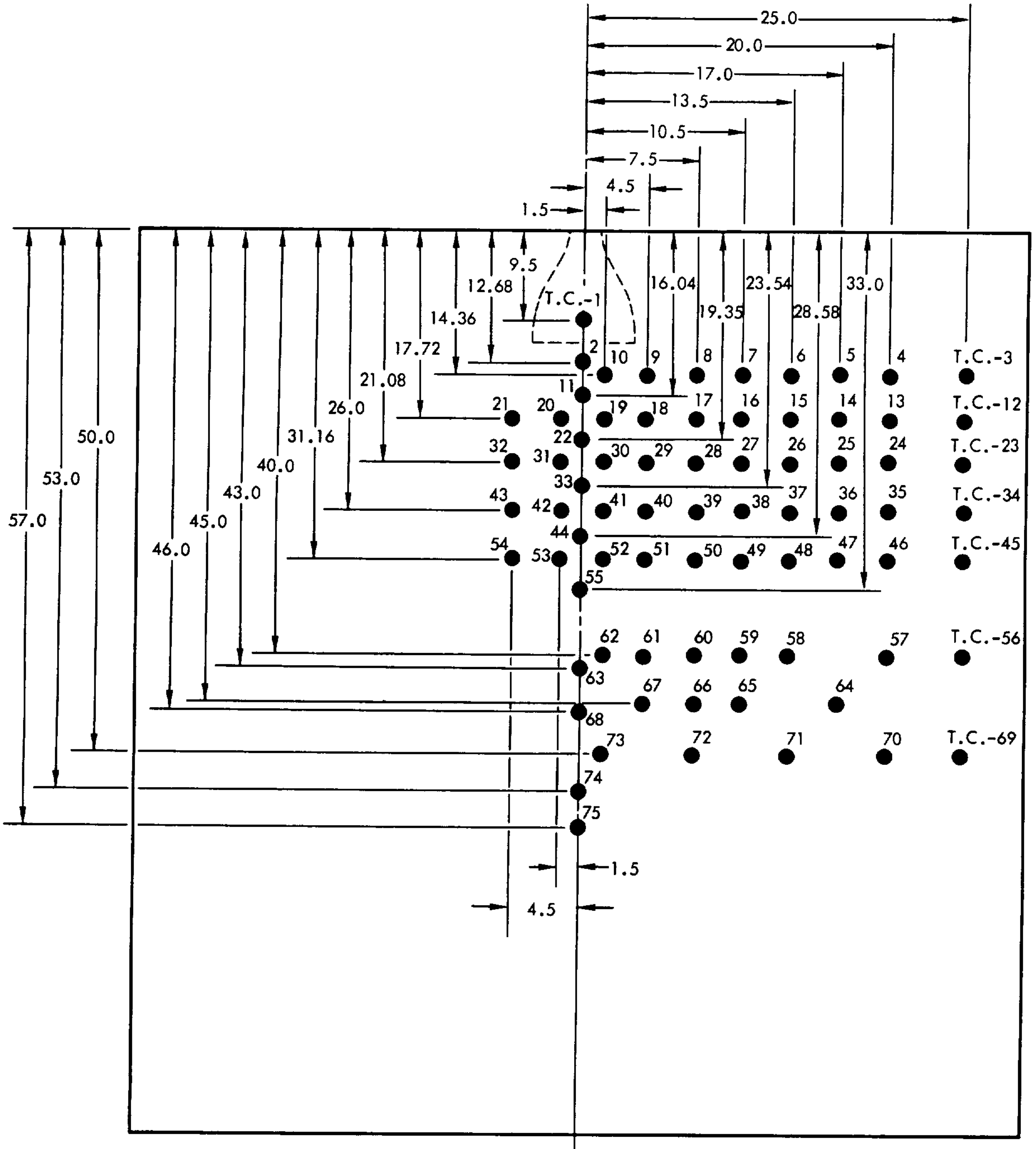
25.0
20.0
17.0
13.5
10.5
7.5
4.5
1.5
9.5
12.68
14.36
17.72
21.08
26.0
31.16
40.0
43.0
45.0
46.0
50.0
53.0
57.0
16.04
19.35
23.54
28.58
33.0
T.C.-1
T.C.-3
T.C.-12
T.C.-23
T.C.-34
T.C.-45
T.C.-56
T.C.-69
2
4
5
6
7
8
9
10
11
13
14
15
16
17
18
19
20
21
22
24
25
26
27
28
29
30
31
32
33
35
36
37
38
39
40
41
42
43
44
46
47
48
49
50
51
52
53
54
55
57
58
59
60
61
62
63
64
65
66
67
68
70
71
72
73
74
75
1.5
4.5
℄

NOTE:

1. ALL DIMENSIONS ARE GIVEN IN INCHES
2. THIS IS A VIEW OF THE FRONT SIDE OF THE IMPINGEMENT PANEL

Figure 9. Thermocouple Locations

SURFACE COATING INSTRUMENTATION, FLAT PLATE

Six one-inch diameter aluminum specimens were inserted into the panel to determine the effect of exhaust constituents on the SM radiator surface. These specimens had the actual radiator coating material, a zinc oxide pigment in a potassium silicate binder (Armour Research Foundation #441-2) applied to the exposed surface and were mounted so that the samples were flush with the stainless sheet. Thermocouples monitored the temperatures of the individual specimens. Figure 10 shows the details of the radiator specimens and the specimen holders. Their locations are shown in Figure 6.

J2A TEST CELL PRESSURE

Although several types of pressure gages (McLeod, Alphatron, Ion, and the variable capacitance type) are used to measure the pressure of the J2A test cell, only the variable capacitance type (Decker 306-2A) is insensitive to the composition of the gas. Since the exact composition of the gas in the test cell during the rocket engine firing is unknown, only the Decker variable capacitance gage cell pressure data is presented as a function of time. This transducer was mounted outside the test cell and was connected to the test cell liner by means of a 0. 5-foot diameter duct. This mounting location was necessary because facilities were not available to accommodate the transducer inside the test cell liner.

ROCKET ENGINE INSTRUMENTATION

The rocket engine flow parameters were fully instrumented. Strain gage type transducers were used for all pressure measurements.

The rocket engine chamber pressure was measured at the injector face. The nozzle exit pressure was measured for the stainless steel nozzles with area ratio of 20:1, 15:1, and 10:1, using a 0. 063-inch tap located 3/16 inch from the nozzle exit plane. The propellants were pressure fed. Propellant pressures were measured at the outlet of the propellant tanks and near the rocket engine propellant valves.

The propellant flow rates were initially obtained with turbine-type flowmeters located just outside the test cell. The oxidizer flowmeter malfunctioned during the area ratio 40:1 runs and was replaced with a Venturi meter on subsequent runs. During the area ratio 20:1 runs, the fuel flowmeter malfunctioned and it too was replaced with a Venturi meter.

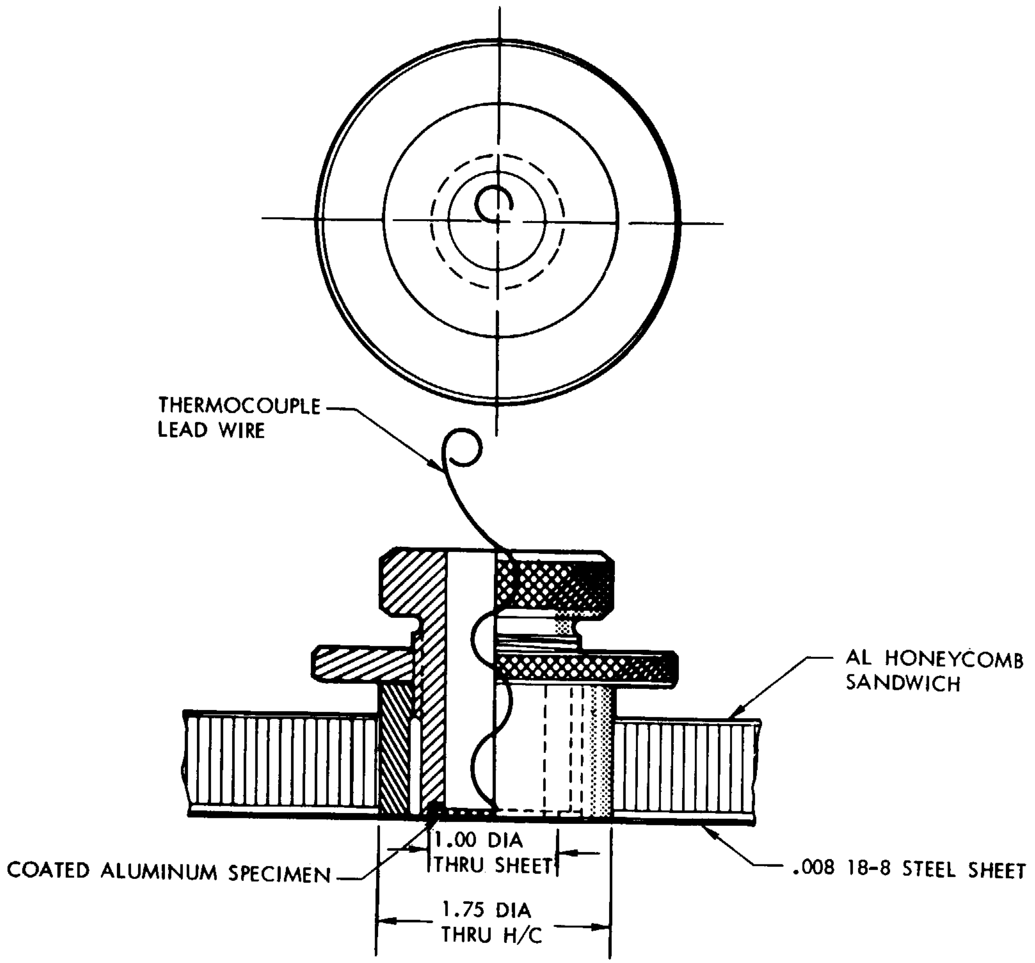
THERMOCOUPLE LEAD WIRE
AL HONEYCOMB SANDWICH
COATED ALUMINUM SPECIMEN
1.00 DIA THRU SHEET
.008 18-8 STEEL SHEET
1.75 DIA THRU H/C

RADIATOR COATING SPECIMEN & HOLDER

Propellant temperatures were measured at the propellant tanks and just downstream of the flowmeters.

The thrust of the rocket engine was not measured.

PHOTOGRAPHIC INSTRUMENTATION

Three 16 mm movie cameras were located in the test cell. Two were positioned normal to and on opposite sides of the rocket engine exhaust centerline. The third 16 mm camera was positioned at an angle to view the exhaust and also the test panel. These camera locations are shown in Figure 3. The film speed was varied from 4 to 16 frames/second for different test runs in an attempt to determine the optimum speed to record the flow visualization. For the 15:1 area ratio run, the third camera was relocated approximately 10 feet downstream of the nozzle exit and was oriented toward the nozzle exit at approximately 30° below the exhaust centerline. The purpose of this relocation was to determine qualitatively the glare that would be encountered by astronauts during a rendezvous. This camera was replaced in its original position for the remaining run.

Closed-circuit television was used for visual monitoring of the rocket engine firings.

III. OPERATING CONDITIONS

TEST CELL

The following description of the J2A test cell operation was abstracted from reference 2.

"The cell annulus and liner (Figure 11) were initially pumped down to approximately 75 mm Hg by means of four mechanical pumps. At this pressure, the valve separating the liner from the annulus was closed and pumping continued on the liner. At a pressure level of approximately 5×10^{-3} torr., liner chilldown with gaseous nitrogen was begun. Incremental temperature changes no greater than 50 K were made to minimize thermal stresses. After a liner temperature of 200 K was reached, the two 20-inch oil diffusion pumps were used to further decrease the pressure. With the test cell at these conditions, the liner was cold enough to freeze any oil backflow from the diffusion pumps. Liner chilldown continued until a temperature of 150 K was reached, and at this point the liner was filled with liquid nitrogen, which reduced the liner temperature to 77 K. Operation of the helium cryoplates was initiated after the liner leak-rate and hardware outgassing decreased to 0.258 atm cc/sec or less. The cryoplates provided a cryopumping surface at approximately 20 K. With the cryoplates chilled to test conditions, the liner pressure stabilized at approximately 2×10^{-5} torr. With the cell at these conditions, altitude calibrations of the instrumentation were taken, and the fuel and oxidizer tanks were pressurized to the desired pre-firing level. A countdown procedure was used during which the operation of different types of recording instrumentation was initiated by an electrical sequencer, and at the end of the countdown the engine firing was initiated. Prior to the next firing, propellant flow rates and mixture ratios were calculated, using the data from the previous run, and were corrected, if required, by adjusting propellant tank pressures. Additional instrumentation calibrations were conducted at regular intervals during testing. The readings of ionization gages were compared with the reading of the McLeod gage down to cell pressure levels of 1×10^{-5} torr. Approximately 30 minutes were required to recover the pre-fire cell pressure level before the next firing could begin."

ROCKET ENGINE

Design operating conditions were requested during the operation of the prototype SM RCS rocket engines. The design fuel flow rate is 0. 11 lbs/sec and the oxidizer flow rate is 0. 22 lbs/sec, which results in an oxidizer-to-fuel ratio of 2. 0. The nominal rocket engine chamber stagnation pressure is 90 psia. The operating conditions of each engine firing were observed and any required changes in the propellant tank pressures were made before the subsequent firing in order to correct the operating conditions.

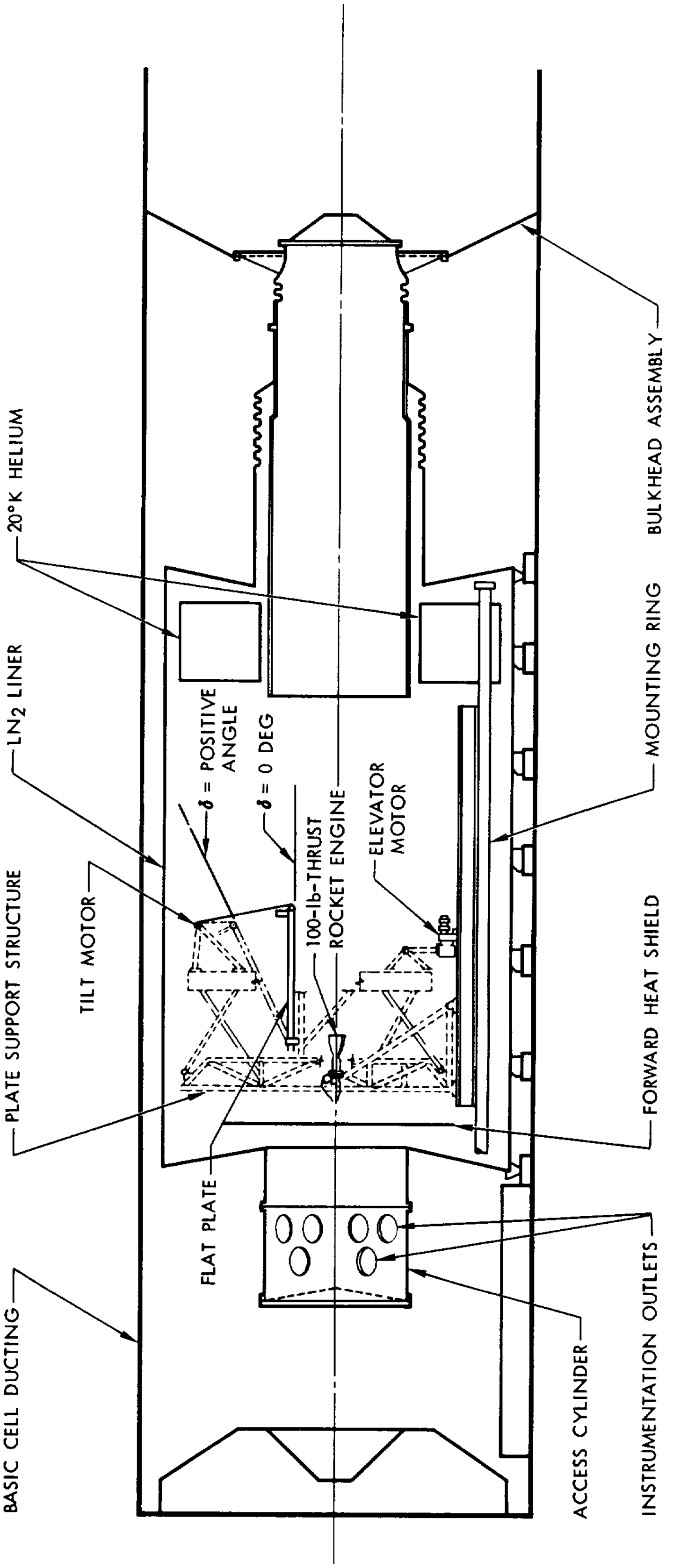
BASIC CELL DUCTING
FLAT PLATE
PLATE SUPPORT STRUCTURE
TILT MOTOR
LN$_2$ LINER
20°K HELIUM
δ = POSITIVE ANGLE
δ = 0 DEG
100-lb-THRUST ROCKET ENGINE
ELEVATOR MOTOR
ACCESS CYLINDER
INSTRUMENTATION OUTLETS
FORWARD HEAT SHIELD
MOUNTING RING
BULKHEAD ASSEMBLY

Figure 11. AEDC J2A Test Cell

IV. TEST PROGRAM

TEST CRITERIA

The primary objectives of the jet plume test were to obtain basic design data and criteria for integrating the SM RCS engines into the Apollo spacecraft system. Data obtained included impingement heating rates and pressure distributions on a flat plate. In addition, the contamination effects of pulsed engine flows on special emissivity coatings and the degree of glare from the engine exhaust were qualitatively determined. The installation geometry will affect all of these considerations and, hence, the test was run parametrically for various nozzle-to-plate elevations and cant angles.

Due to the uncertainties in the analytical techniques for predicting and extrapolating impingement heat transfer or pressure data, a full-scale test was performed. At this writing, no published experimental data are available to determine the validity of theoretical heat transfer predictions due to exhaust impingement at very low ambient pressures.

TEST CONDITIONS

Tests were performed for various nozzle-to-plate elevations (3 to 15 nozzle exit radii) and the cant angles (0 to 35 degrees). The coordinate system used in this program is shown in Figure 12. Note that the relative location of the instrumentation shifts with the cant angle of the plate; for each cant angle, the shift is a constant value.

A run schedule for each area ratio nozzle is given in Table I. Each test point (rocket engine firing) was approximately two seconds in duration. During this time the test cell pressure altitude varied from approximately 400,000 feet to 200,000 feet.

The testing procedure is described in reference 2, which reports the feasibility program conducted in conjunction with, but prior to, the present program.

The rocket engine propellant flow rates, mixture ratio, engine chamber pressure at the injector, and the nozzle exit pressure are given for each data point in Table 1.

Preceding page blank

Table 1. Test Run Schedule

Data Point	Plate Elevation h (Re)	Plate Cant Angle δ(deg)	Fuel Flow Rate (lb/sec)	Oxidizer Flow Rate (lb/sec)	Mixture Ratio MR	Injector Face Chamber Pressure P_c (psia)	Exit Pressure P_{ex}(psia)	Firing Time (sec)
	ϵ = 40:1			Run -01				
20	10.7	0	.1143	No Data		98	Not Instrumented	2.00
21	10.7	0	.1215			99		1.96
22	10.7	0	.1103			97		2.09
23	10.7	0	.1080			97		2.00
24	10.7	0	.1098			98		2.02
35	3.0	0	.1098			97		1.93
36	3.0	0	.1134			98		1.95
37	7.0	0	.1139			97		1.94
38	7.0	0	.1103			97		2.02
39	10.7	0	.1103			98		1.80
40	10.7	0	.1114			98		1.82
	ϵ = 40:1			Run -01A				
20	3.0	0	.113	.241	2.13	97	Not Instrumented	2.12
21	3.0	0	.116	.235	2.04	97		2.02
22	3.0	10	.112	.238	2.13	96		2.03
23	3.0	10	.112	.237	2.12	97		2.04
24	3.0	15	.112	.237	2.11	96		2.01
25	3.0	15	.114	.237	2.08	97		1.99
36	3.0	25	.128	.236	1.84	96		2.00
37	3.0	25	.110	.239	2.17	97		2.07
38	3.0	35	.109	.237	2.18	96		1.93
39	3.0	35	.116	.237	2.04	96		2.07
40	7.0	0	.111	.234	2.10	97		2.10
41	7.0	15	.116	.235	2.03	101		1.99
42	7.0	25	.105	.235	2.23	96		2.17
53	10.7	0	.114	.240	2.11	96		2.02
54	10.7	15	.116	.234	2.02	96		2.03
55	10.7	15	.112	.234	2.09	96		2.07
56	10.7	0	.112	.235	2.09	96		2.22
57	7.0	0	.113	.235	2.08	95		2.20
58	7.0	15	.116	.229	1.98	96		2.20
59	7.0	25	.113	.230	2.03	96		2.20
	ϵ = 20:1			Run -02				
20	3.0	0	.119	.247	2.08	95	.69	2.04
21	3.0	0	.111	.245	2.21	96	.73	1.93
22	3.0	15	.111	.241	2.18	95	.72	2.07
23	3.0	15	.111	.241	2.17	95	.73	2.13
24	3.0	25	.110	.241	2.20	96	.73	2.24
25	3.0	25	.110	.240	2.18	96	.73	2.17
36	7.0	0		No Data		96	.73	2.22

Table 1. Test Run Schedule (Cont)

Data Point	Plate Elevation h (Re)	Plate Cant Angle δ (deg)	Fuel Flow Rate (lb/sec)	Oxidizer Flow Rate (lb/sec)	Mixture Ratio MR	Injector Face Chamber Pressure P_c (psia)	Exit Pressure P_{ex} (psia)	Firing Time (sec)
37	7.0	15		No Data		97	.73	2.17
38	7.0	25				96	.72	1.99
39	7.0	35				96	.72	2.12
40	11.0	0				96	.73	2.17
41	11.0	15				96	.73	2.07
42	11.0	25				96	.73	2.13
43	11.0	35				95	.70	2.23
54	11.0	35				96	.72	2.10
55	15.0	0				96	.65	2.17
56	15.0	0		Ran out of propellant		35	.25	2.12
	ϵ = 15:1			Run -03				
20	12.8	35	.102	.249	2.44	92	.93	2.00
21	↓	35	.103	.244	2.37	93	.93	2.00
22		25	.106	.244	2.30	93	.94	2.00
23		25	.106	.237	2.24	91	.94	2.00
24		15	.106	.224	2.11	91	.93	1.97
25		15	.109	.221	2.02	91	.93	1.92
26		0	.109	.221	2.02	91	.94	1.83
27	12.8	0	.110	.221	2.01	92	.93	1.90
38	9.0	35	.102	.211	2.07	91	.93	1.95
39	↓	35	.101	.208	2.06	91	.93	1.95
40		25	.110	.220	2.00	91	.93	2.06
41		25	.110	.220	2.00	91	.93	2.03
42		15	.104	.213	2.04	91	.93	1.96
43		15	.110	.221	2.00	91	.93	1.88
44		0	.110	.221	2.00	91	.94	2.08
45	9.0	0	.110	.221	2.00	91	.96	2.04
57	7.0	35	.111	.223	2.00	91	.95	1.99
58	↓	35	.101	.222	2.20	91	.96	2.08
59		25	.110	.217	1.97	91	.96	2.50
60		25	.107	.222	2.07	91	.95	1.97
61		15	.110	.222	2.02	91	.96	2.03
62		15	.109	.221	2.04	91	.96	2.00
63		0	.109	.222	2.04	91	.95	2.22
64	7.0	0		No Data		91	.95	2.00
76	5.0	35	.110	.221	2.01	92	.95	2.04
77	↓	35	.110	.221	2.01	91	.96	2.00
78		25	.110	.221	2.01	91	.96	2.06
79		25	.110	.221	2.01	91	.96	2.10
80		15	.110	.221	2.01	91	.95	2.04
81		15	.110	.220	2.00	91	.95	2.05
82		0	.110	.221	2.01	92	.96	1.90
83		0	.110	.222	2.02	91	.95	1.99
84	5.0	0	.104	.222	2.07	—	.96	2.04

Table 1. Test Run Schedule (Cont)

Data Point	Plate Elevation h (Re)	Plate Cant Angle δ (deg)	Fuel Flow Rate (lb/sec)	Oxidizer Flow Rate (lb/sec)	Mixture Rate MR	Injector Face Chamber Pressure P_c (psia)	Exit Pressure P_{ex} (psia)	Firing Time (sec)
ϵ = 10:1		Run -04						
58	11.0	35	.115	.188	1.63	83	No Data	1.91
59		35	.112	.200	1.78	85		1.98
60		25	.113	.194	1.70	84		1.92
61		25	.113	.200	1.78	86		1.93
62		15	.106	.198	1.86	87		1.96
63		15	.112	.207	1.85	89		2.00
64		0	.114	.210	1.84	89		2.04
65	11.0	0	.109	.206	1.88	88		2.03
76	7.0	35	.108	.226	2.10	90		2.06
77		35	.107	.222	2.07	90		2.13
78		25	.109	.221	2.02	90		1.94
79		25	.110	.225	2.04	90		1.99
80		15	.109	.223	2.04	90		2.17
81		15	.110	.224	2.05	90		2.01
82		0	.109	.224	2.05	90		2.04
83		0	.109	.224	2.05	90		2.03
95		0	.109	.216	1.98	88		2.15
96	7.0	0	.111	.221	2.00	89		2.06
ϵ = 10:1		Run -04A						
20	5.0	35	.104	.218	2.09	88	1.62	2.01
21		35	.110	.208	1.89	89	1.62	1.94
22		25	.110	.207	1.87	—	1.62	2.02
23		25	.109	.206	1.89	89	1.64	2.00
24		15	.109	.209	1.92	89	1.64	2.03
25		15	.109	.207	1.90	89	1.64	1.93
26		0	.108	.208	1.93	89	1.62	2.06
27	5.0	0	.110	.212	1.93	89	1.64	2.01
38	3.0	35	.108	.195	1.80	89	1.66	2.04
39		35	.109	.206	1.90	89	1.69	2.03
40		25	.110	.213	1.94	89	1.67	2.01
41		25	.112	.217	1.95	88	1.67	2.05
42		15	.111	.217	1.95	88	1.68	2.10
43		15	.109	.215	1.96	89	1.68	2.02
44		0	.109	.229	2.10	89	1.68	2.05
45	3.0	0	.110	.215	1.96	88	1.68	2.10
56	9.0	35	.110	.215	1.96	88	1.64	2.06
57		35	.108	.215	1.99	88	1.65	1.92
58		25	.100	.214	2.14	89	1.63	2.16
59		25	.109	.215	1.98	88	1.64	2.10
60		15	.111	.216	1.94	90	1.68	2.19
61	9.0	15	.111	.216	1.94	90	1.66	2.14

Table 1. Test Run Schedule (Cont)

Data Point	Plate Elevation h (Re)	Plate Cant Angle δ(deg)	Fuel Flow Rate (lb/sec)	Oxidizer Flow Rate (lb/sec)	Mixture Rate MR	Face Chamber Pressure P_c (psia)	Exit Pressure P_{ex} (psia)	Firing Time (sec)
62	9.0	0	.113	.216	1.91	91	1.68	2.00
63	9.0	0	.113	.215	1.91	91	1.68	2.20
74	13.0	35	.111	.221	1.99	92	1.70	2.00
75	↓	35	.113	.220	1.95	92	1.68	2.20
76		25	.112	.221	1.98	92	1.70	2.00
77		25	.112	.221	1.98	92	1.68	2.00
78		15	.116	.228	1.97	92	1.69	1.97
79		15	.113	.224	1.98	91	1.66	2.00
82		0		No Data		90	1.66	2.00
84	13.0	0		↓		90	1.65	2.18
85	17.5	0				90	1.65	2.19
86	17.5	0				90	1.70	10.28

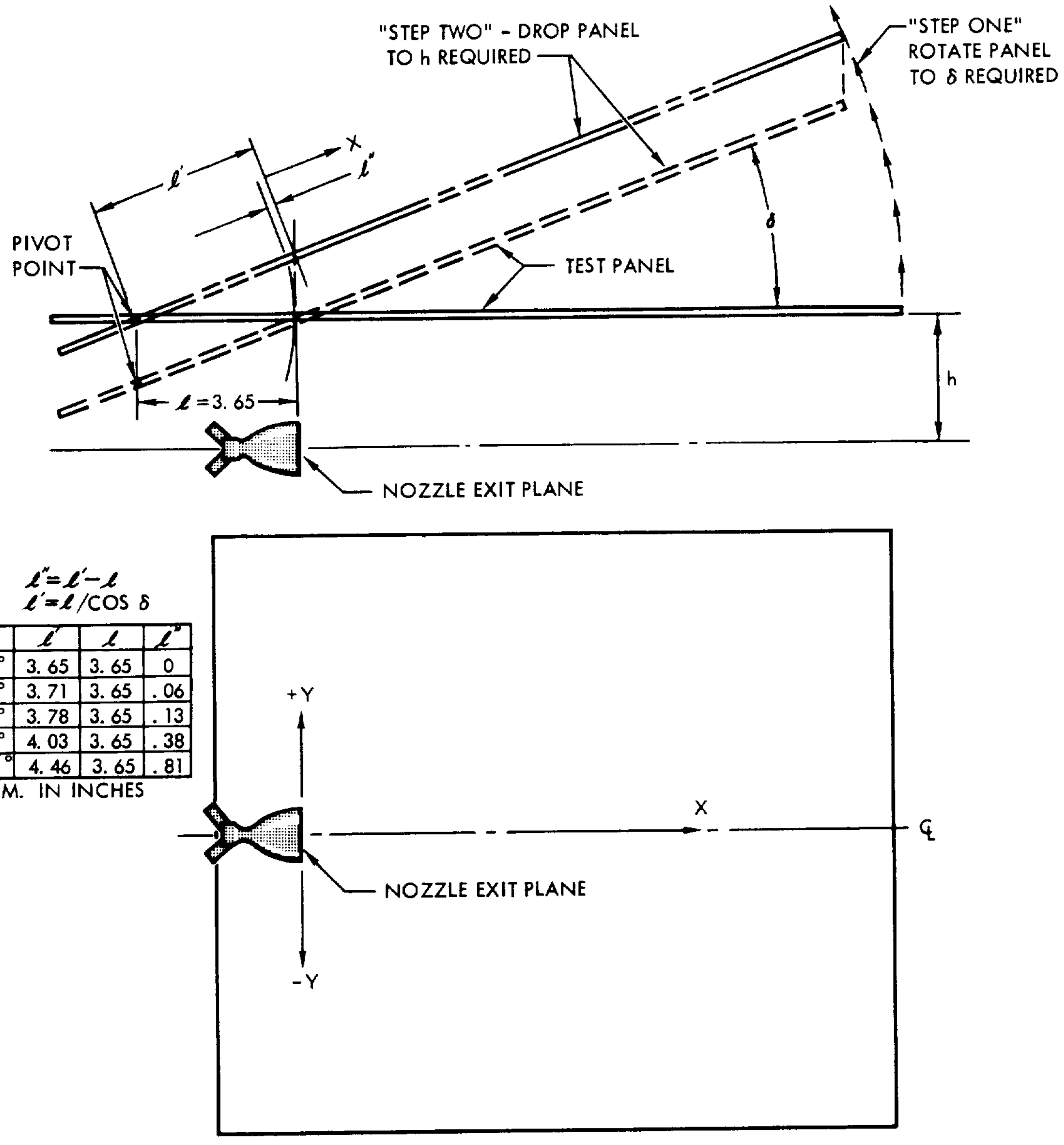
"STEP TWO" - DROP PANEL TO h REQUIRED
"STEP ONE" ROTATE PANEL TO δ REQUIRED
X
ℓ''
ℓ'
δ
PIVOT POINT
TEST PANEL
h
ℓ = 3.65
NOZZLE EXIT PLANE
+Y
X
℄
NOZZLE EXIT PLANE
-Y

$\ell'' = \ell' - \ell$

$\ell' = \ell / \cos\delta$

δ	ℓ'	ℓ	ℓ''
0°	3.65	3.65	0
10°	3.71	3.65	.06
15°	3.78	3.65	.13
25°	4.03	3.65	.38
35°	4.46	3.65	.81

DIM. IN INCHES

X = DISTANCE ON FLAT PLATE FROM INTERSECTION OF NOZZLE EXIT PLANE.
Y = DISTANCE ON FLAT PLATE FROM NOZZLE CENTER LINE PROJECTION TO PLATE.
h = DISTANCE TO FLAT PLATE FROM NOZZLE AXIS IN NOZZLE EXIT PLANE.
δ = CANT ANGLE BETWEEN NOZZLE CENTER LINE AND PLATE.
ℓ = DISTANCE FROM EXIT PLANE TO PIVOT AT $\delta = 0°$
ℓ' = DISTANCE FROM EXIT PLANE TO PIVOT AT $\delta < 0°$
ℓ'' = INSTRUMENTATION SHIFT.

Figure 12. Coordinate System

Typical plume expansion pressure ratios, Pc/P_∞, varied between 1×10^8 and 1×10^4 during the engine firing. The test cell pressure-altitude versus time variation is shown in Figure 13.

HEATING RATE DATA REDUCTION

Theoretical exhaust flow field calculations by the method of characteristics show that the properties inside of highly expanded plume boundary shocks do not vary over a change of several orders of magnitude in ambient pressure for a given rocket engine. If it can be assumed that impingement properties do not vary for this same region when there is an interfering surface, the heating rates and surface pressure will be a constant value with changing altitude.

In the present test program, ambient pressure is very low (10^{-6} to 10^{-3} psia); the total to ambient pressure ratio is very high (10^8 to 10^4). Thus the flow in the plume is hypersonic and Newtonian flow approximations should apply.

Because of the above, it was expected that for the entire range of test cell pressure, the surface pressures and the heating rates would be constant values at each measurement point, as long as the boundary region did not interfere.

In order to determine the approximate area of plume impingement on the flat plate that would be outside the influence of the boundary region, the plume (using flow visualization movies) was graphically plotted on the flat plate as a function of time. A typical example is Figure 14. For those instrumentation points that were well inside this boundary at the end of the firing, the entire firing time (Δt) and the entire temperature rise (ΔT) during this time could be used to determine the heating rate in the thin skin equation:

$$q = \rho \delta C_p \frac{\Delta T}{\Delta t} \tag{1}$$

q = heating rate BTU/ft^2/sec

ρ = skin density 504.2 lb/ft^3

δ = skin thickness 0.000666 ft (.008 inches)

C_p = skin heat capacity at $\frac{T_2 + T_1}{2}$ (See Figure 15.)

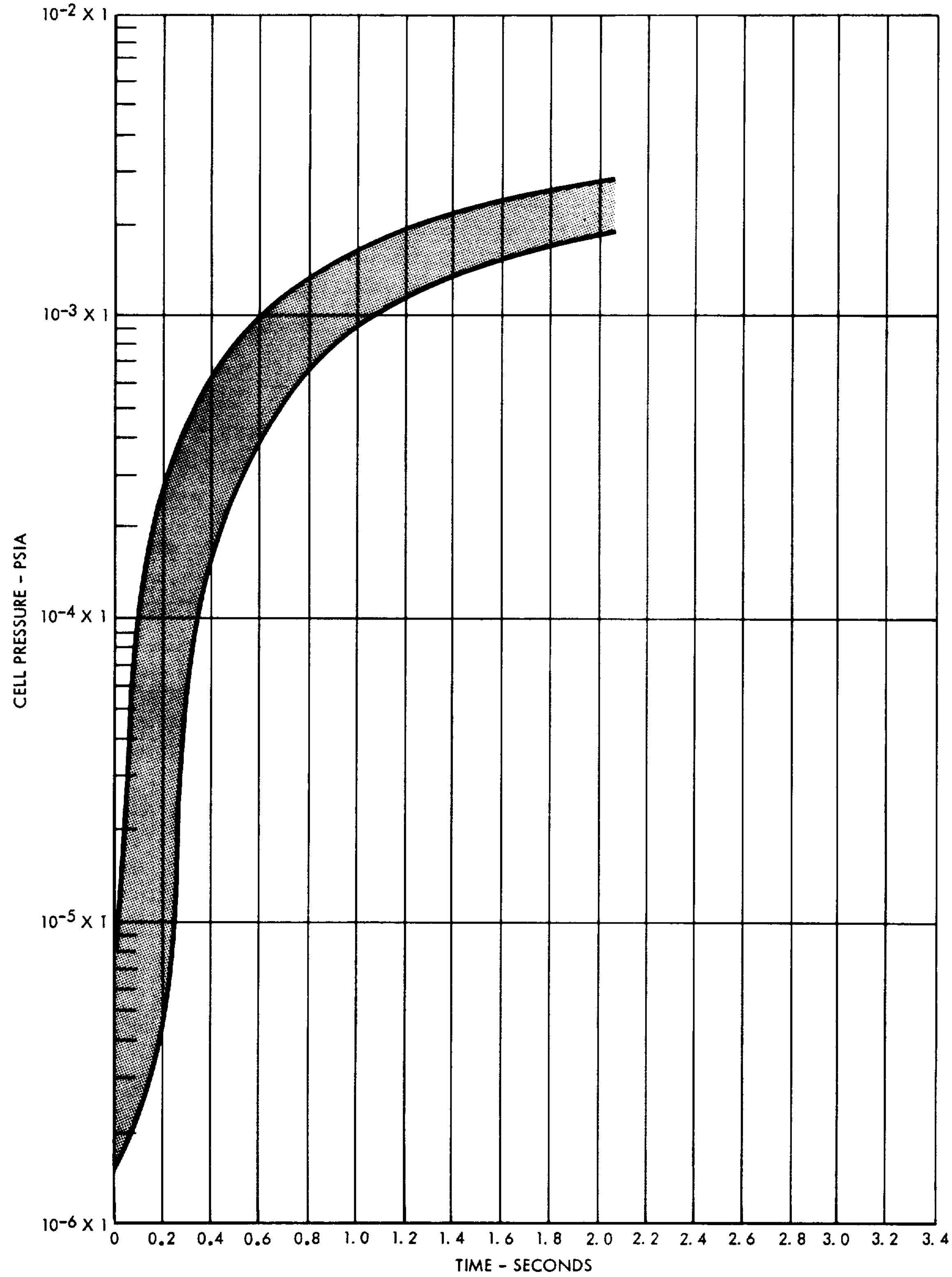

Figure 13. Ambient Pressure - Time Variation of the J2A Test Cell

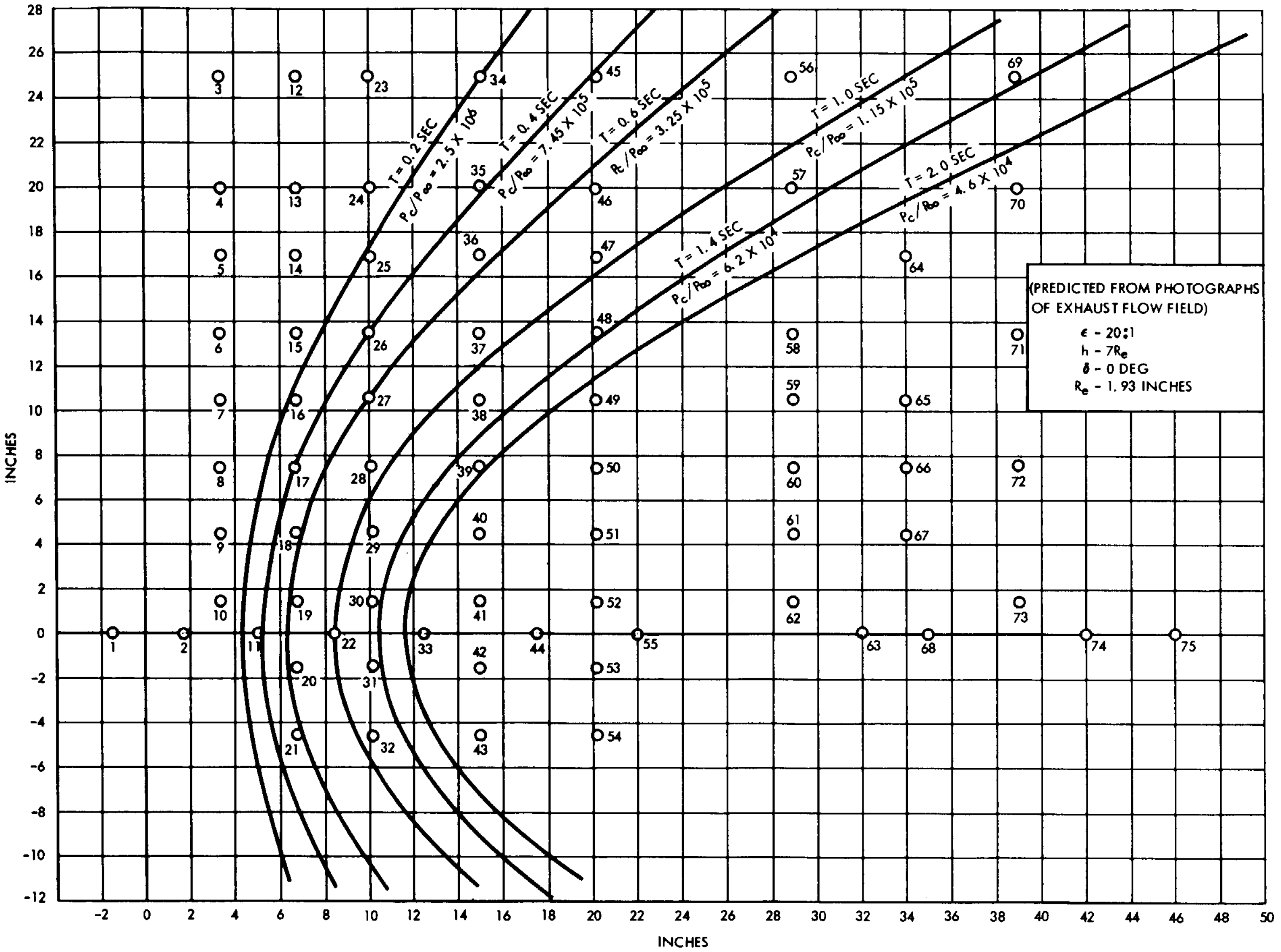

Figure 14. Plume Boundary Profiles on Impingement Panel

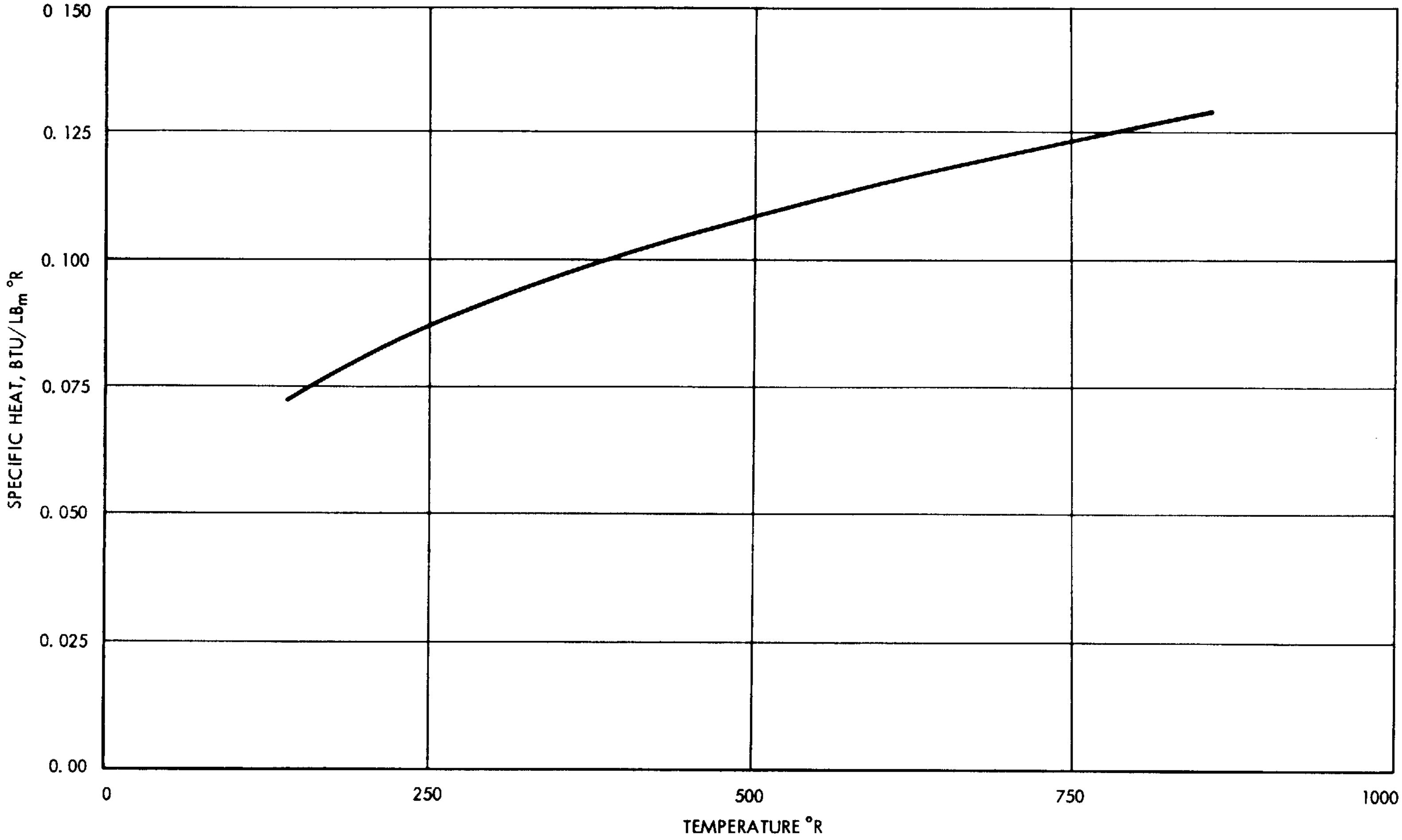

SOURCE: THERMOPHYSICAL PROPERTIES OF SOLID MATERIAL VOL. II, WADC TECHNICAL REPORT NO. 58-476

Figure 15. Specific Heat Versus Temperature for 18-8 Stainless Steel

Typical temperature-time histories for this region are given in Figures 16 through 19. It can be seen from the figures that the slope of the curves decreases slightly with time. If the heating rate is constant, it would be expected that the slope of the temperature curve would decrease, since the surface heat capacity increases with temperature.

For those instrumentation points over which the exhaust boundary region does pass during the engine firing time, the temperature-time histories were plotted for each location. Typical temperature histories for these points are given in Figure 20. These graphs have very definite inflection points followed by an increased slope of the curve. The higher heating rate (steeper temperature gradient) in this region is attributed to the lower Mach number (higher density) flow between the plume boundary and the interior boundary shock. It is expected that continuing analysis will show that the boundary region is passing through the instrumented point during this time. Only the temperature history before the inflection point was used to determine the heating rates for this region.

Figure 21 shows typical repeatability of the data for this test. It is seen that the slope of this thermocouple is nearly the same for the four different firings at the same configuration.

Finally, the pressure time histories presented in Figure 22 indicate that the surface pressure does not vary with ambient pressure (time). It should be noted that these data show the typical invariance of the surface pressure level with time of all the pressure data obtained inside the exhaust boundary region.

DATA REDUCTION AND DATA ACCURACY

Heating rates are obtained from the thin-skin equation (1). Temperature data was obtained thirty times a second, but printed out only ten times a second.

The accuracy of the heating rates presented depends upon the model configuration, the accuracy of the heat capacity value, the density of the thin skin, and the thickness of the thin skin. The accuracy of the actual temperature is ± six percent; ± three percent is due to instrumentation and ± three percent is due to the recording system at AEDC. The variation in the initial temperature of the various thermocouples is due to the heating elements near the pressure transducers. These initial temperatures were in equilibrium prior to each rocket engine firing, so no error is involved. Since a temperature differential is used in Equation (1), the

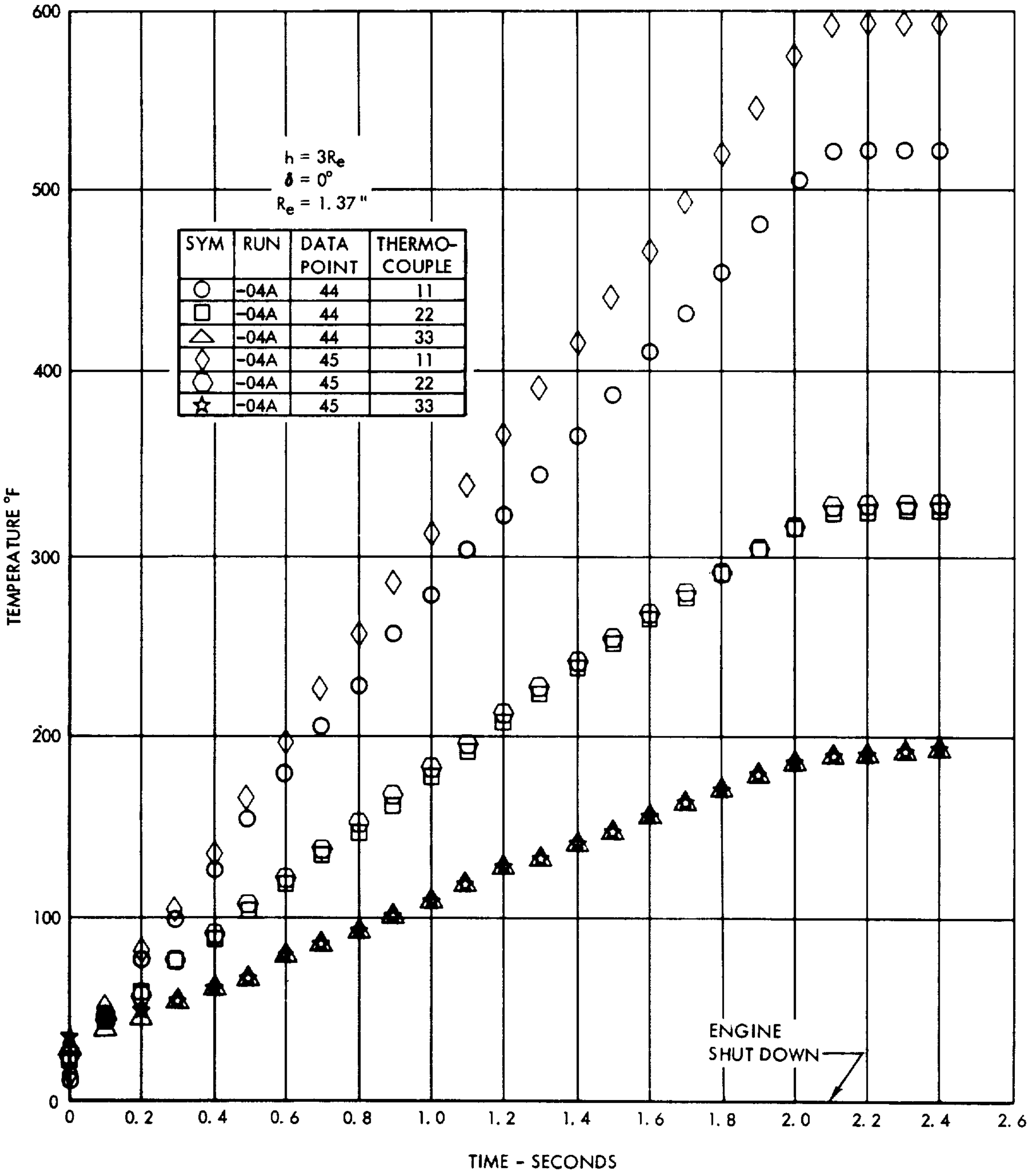

Figure 16. Temperature - Time Histories ϵ = 10:1 (Thermocouples Undisturbed by Boundary Region)

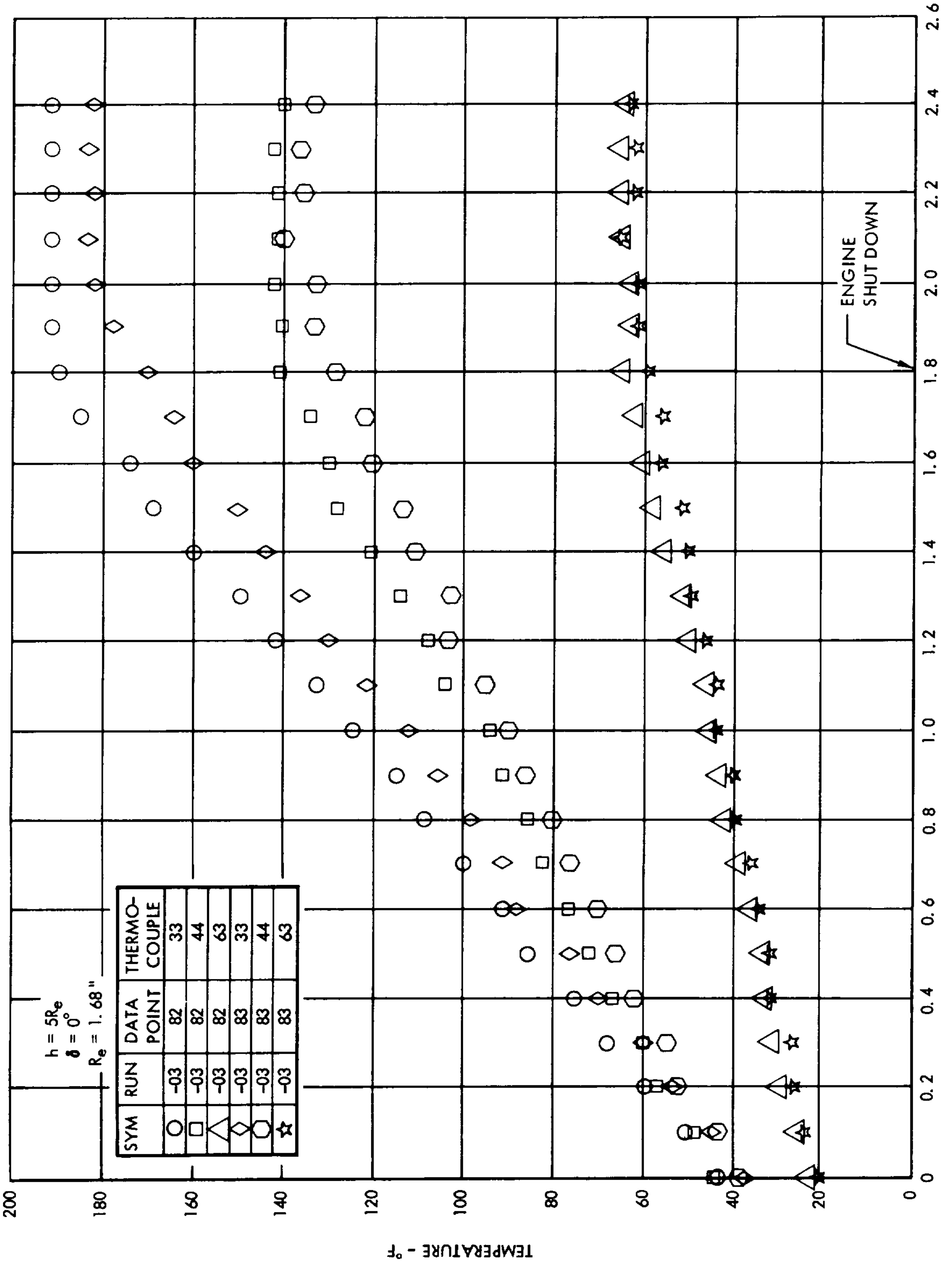

Figure 17. Temperature - Time Histories $\epsilon = 15{:}1$ (Thermocouples Undisturbed by Boundary Region)

$h = 3R_e$
$\delta = 0°$
$R_e = 1.94''$

SYM	RUN	DATA POINT	THERMO-COUPLE
○	-02	20	11
□	-02	20	22
△	-02	20	33
◇	-02	21	11
⬡	-02	21	22
☆	-02	21	33

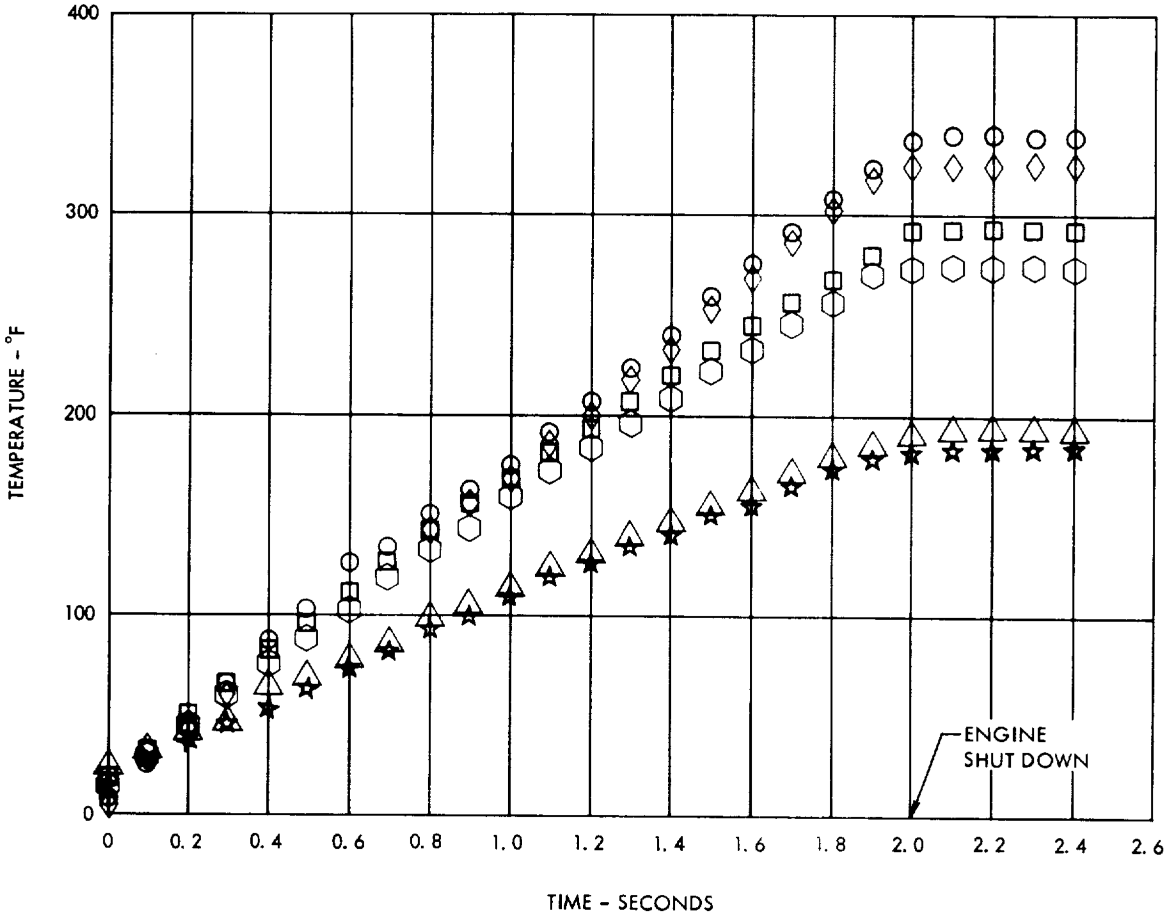

Figure 18. Temperature - Time Histories $\epsilon = 20:1$ (Thermocouples Undisturbed by Boundary Region)

$h = 3R_e$
$\delta = 0°$
$R_e = 2.73''$

SYM	RUN	DATA POINT	THERMO-COUPLE
○	-01	20	33
□	-01	20	44
△	-01	20	63
◇	-01	21	33
⬡	-01	21	44
☆	-01	21	63

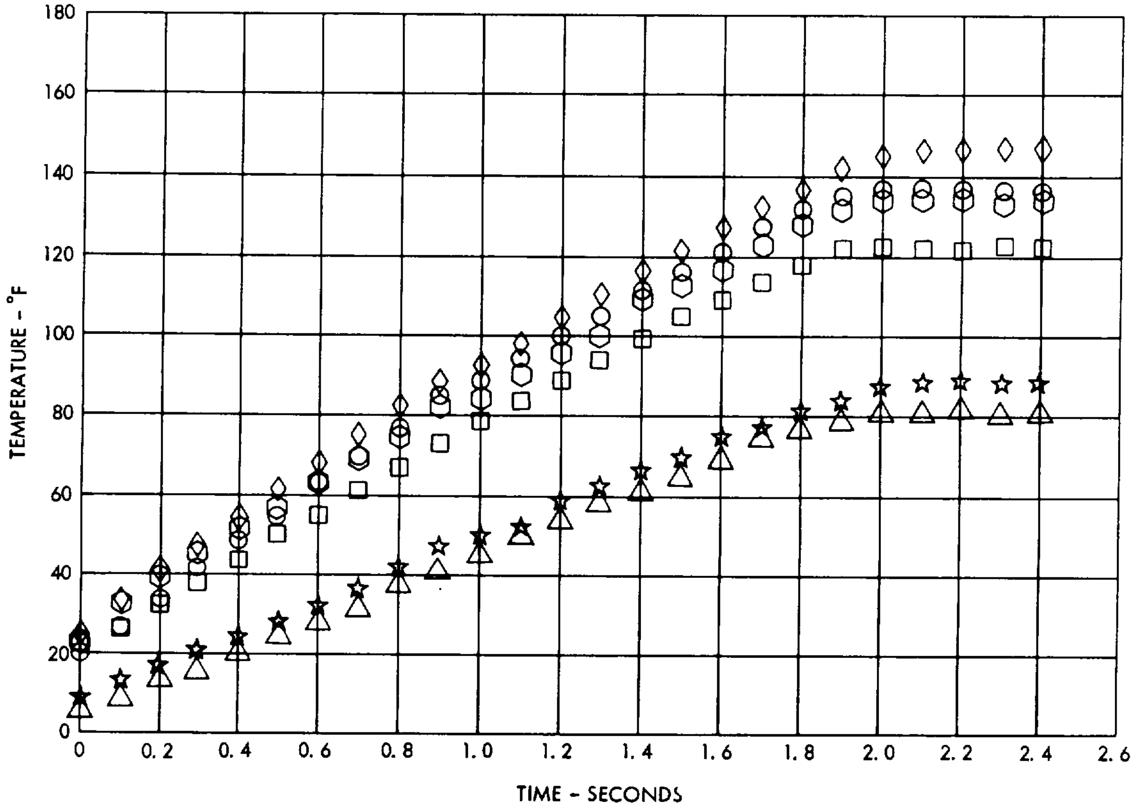

Figure 19. Temperature - Time Histories $\epsilon = 40:1$ (Thermocouples Undisturbed by Boundary Region)

$h = 3R_e$
$\delta = 0^\circ$
$R_e = 2.73''$

SYM	RUN	DATA POINT	THERMO-COUPLE
○	-01	35	36
□	-01	35	37
△	-01	35	38
◇	-01	35	39

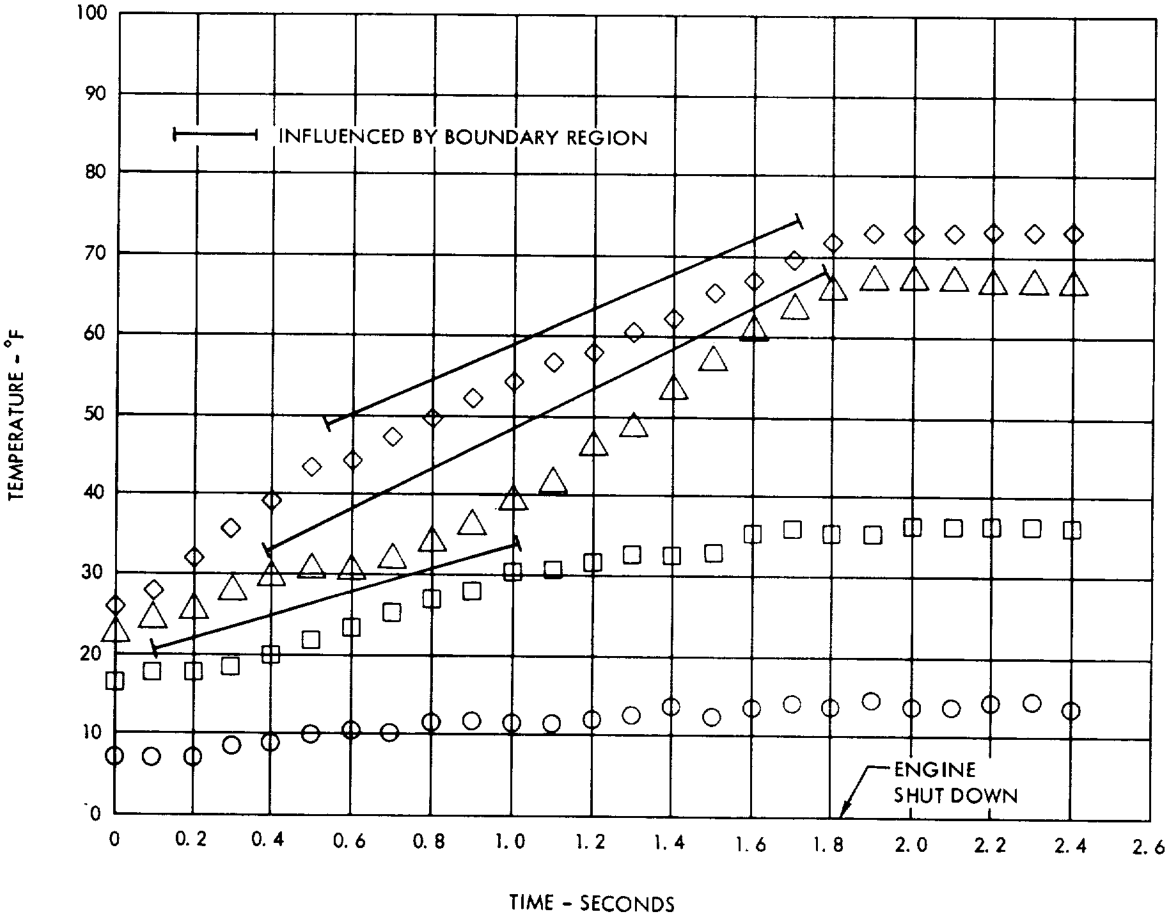

Figure 20. Temperature - Time Histories ϵ = 40:1 (Thermocouples Influenced by Boundary Region)

$h = 3R_e$
$\delta = 0°$
$R_e = 2.73"$

SYM	RUN	DATA POINT	THERMO-COUPLE
◇	-01	35	33
⬡	-01	36	33
△	-01A	20	33
○	-01A	21	33

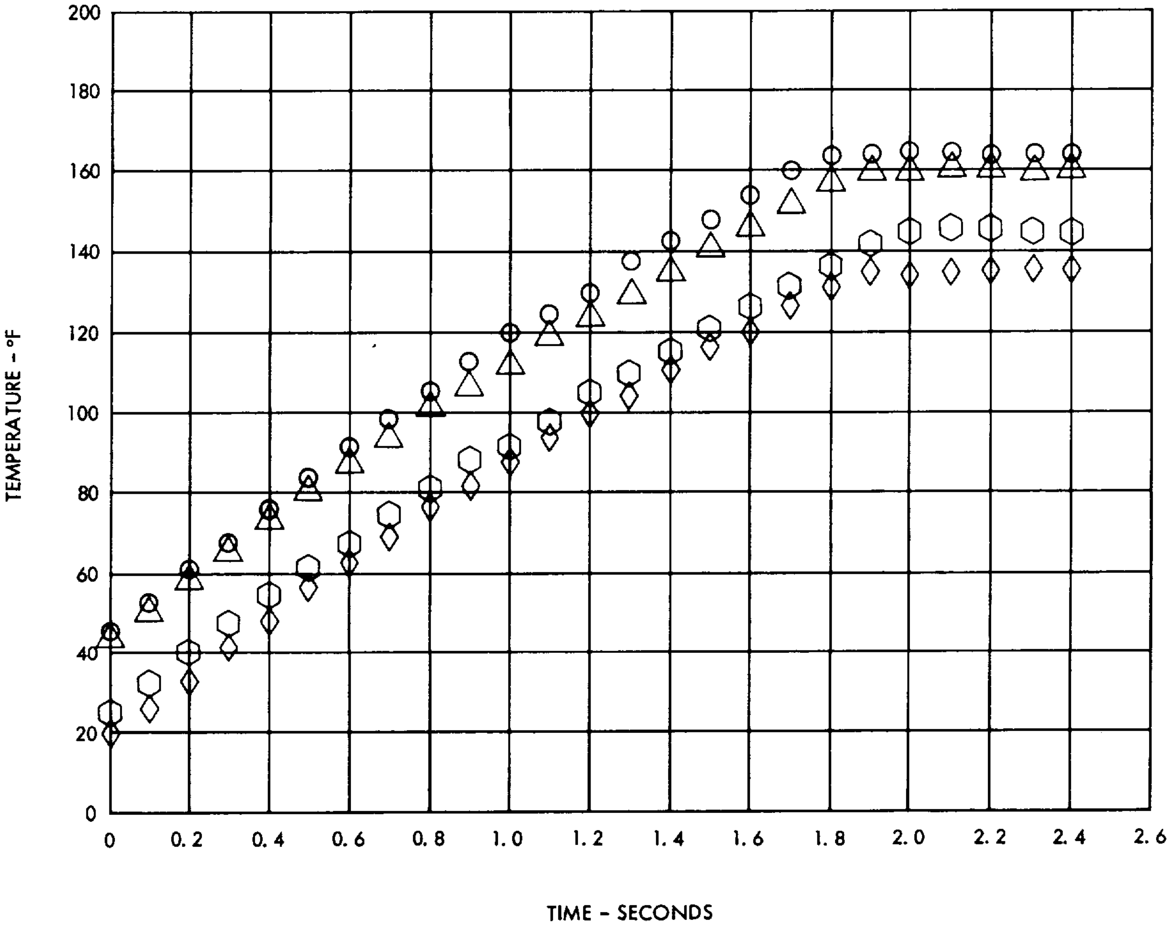

Figure 21. Temperature - Time Histories $\epsilon = 40:1$ (Typical Data Repeatability)

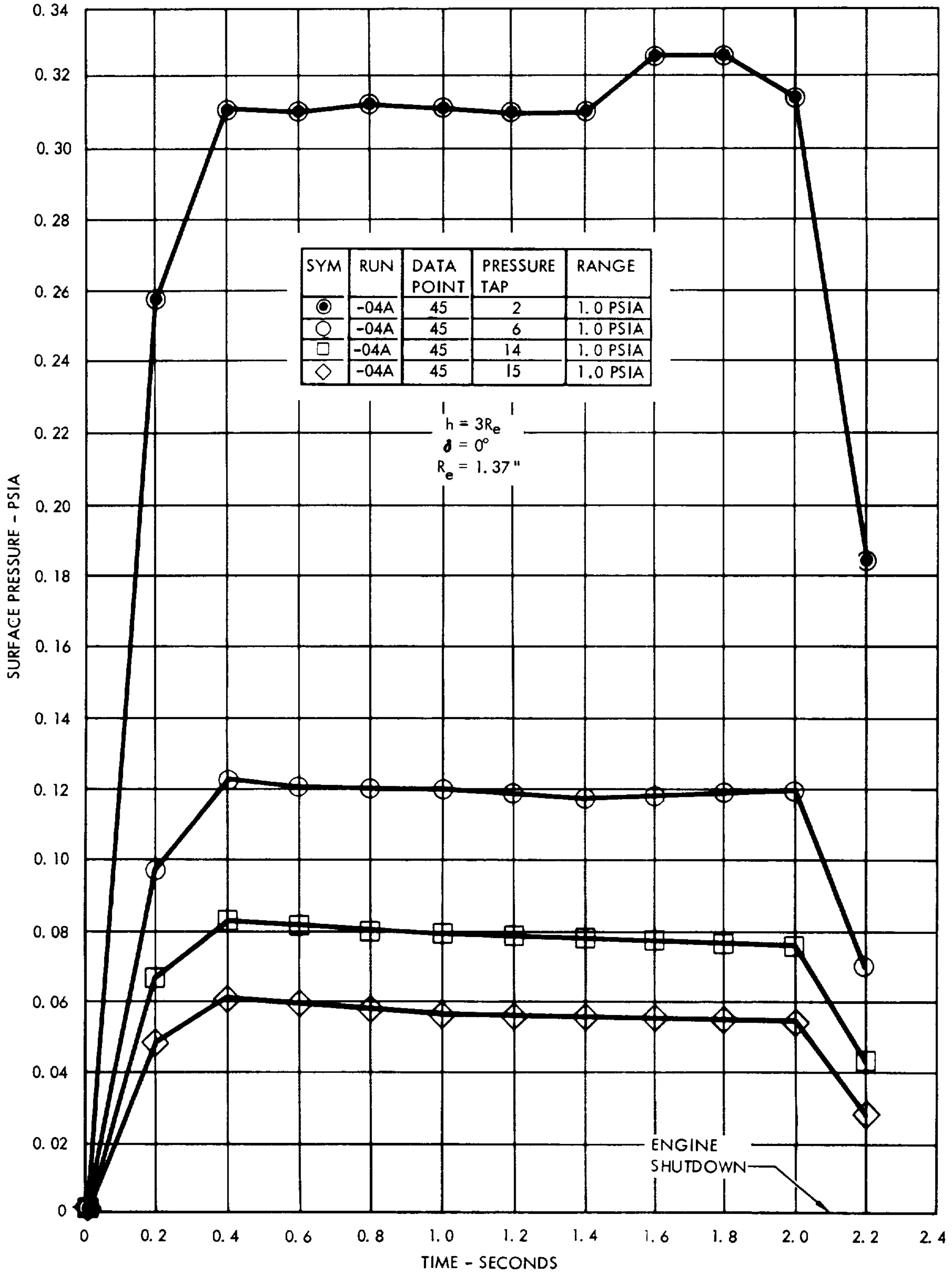

Figure 22. Surface Pressure - Time Histories $\epsilon = 10:1$

accuracy of the temperature will only affect the value of the heat capacity chosen. The heat lost because of tangential conduction in the skin, and the thermocouple wire conduction was found, from reference 4, to be less than one percent. The temperature through the skin is essentially constant, (reference 4). Convection losses are negligible because the back side of the skin is at near-vacuum cell pressure. Radiation losses are negligible because temperature differences from the surrounding structure are at maximum only a few hundred degrees.

The error in the heat capacity value of 18-8 stainless steel, Figure 15, is not known, but is expected to be small. The error in the density of the material is negligible. From measurement of the thickness of the 18-8 stainless steel sheet used, the accuracy of the 0.008 inches used in the calculation is ±2 percent. Two tests were made at nearly all configurations to check for repeatability of the data; (for one configuration four tests were made; see Figure 21). As is evident from the data presented in this report, the repeatability is very good.

Since the temperature-time thermocouple data does not fall exactly on a straight line, the choice of slope will affect the heating rates. An average slope was chosen, but the range of possible slopes is only about ±5 percent. Considering all of the above, the maximum error for this test is less than ±10 percent or 0.1 BTU/ft^2/sec, whichever is greater.

TEST RESULTS

Heating rate data and surface pressure on the flat plate due to exhaust impingement were obtained during the engine firings as the pressure altitude varied with time. Part of the data obtained in this program is presented in this report. The remainder of the data along with theoretical correlation will be presented in a later report.

The heating rate data distribution for the centerline of the flat plate and one distribution perpendicular to the centerline are presented for eight different variations of nozzle area ratio and stand-off distance at zero nozzle cant angle. These data are presented in Figures 23 to 30. In addition, the complete set of heating rate data obtained from this program is presented for the Apollo design condition for the SM RCS. For this design condition, the centerline of the nozzle at the nozzle exit is three nozzle exit radii from the plate, and the nozzle-axis-to-plate angle is 10 degrees. These data are presented in Figures 31 through 34. These data may be used for the Apollo SM RCS pitch engine design, since a flat plate closely approximates the curvature of the SM surface and the data presented will not vary in space. A heating rate map, on the flat plate surface, based on these data is presented in Figure 35. At the point where the minimum heating rate

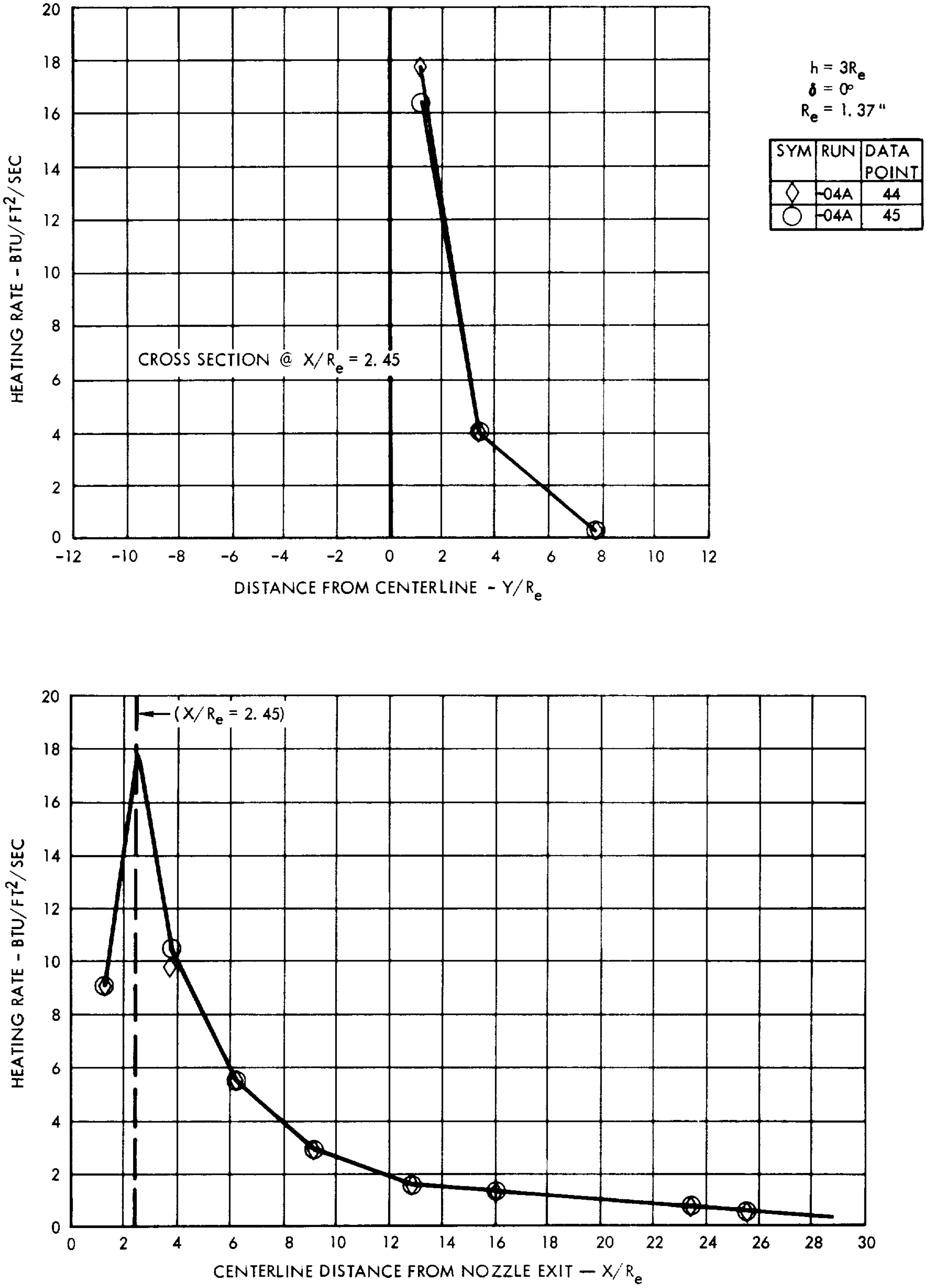

Figure 23. Heating Rate Distribution ϵ = 10:1

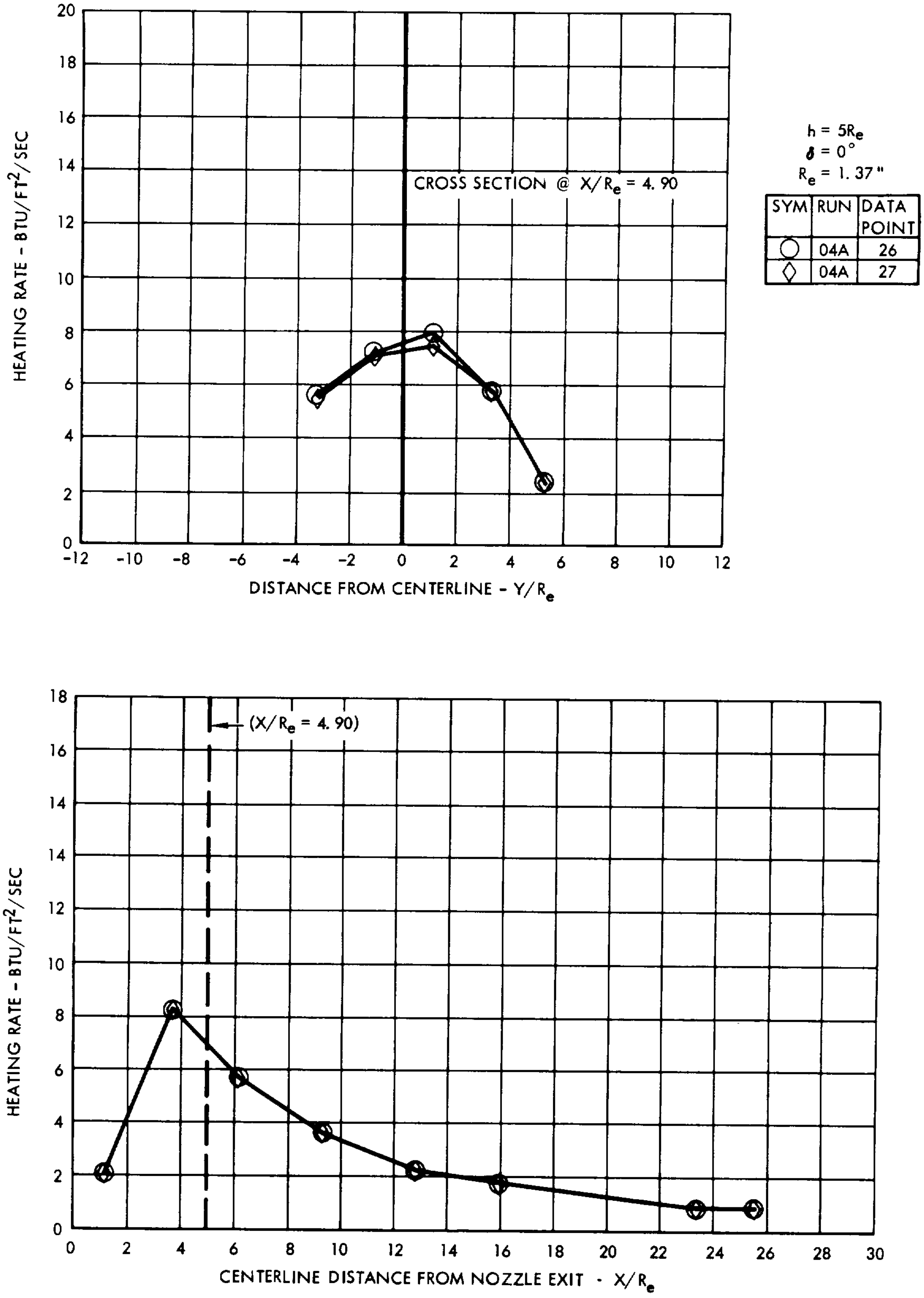

Figure 24. Heating Rate Distribution ϵ = 10:1

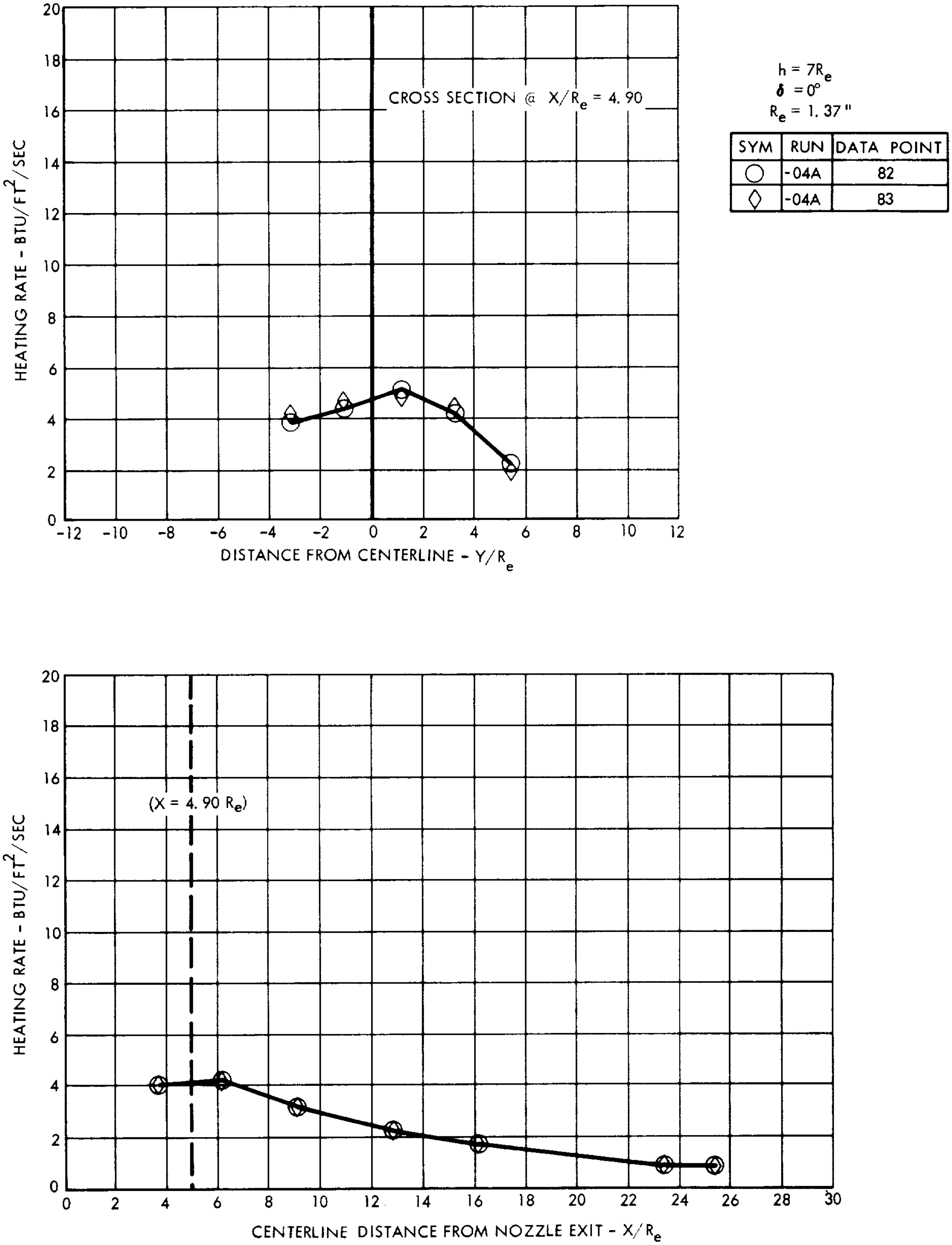

Figure 25. Heating Rate Distribution ϵ = 10:1

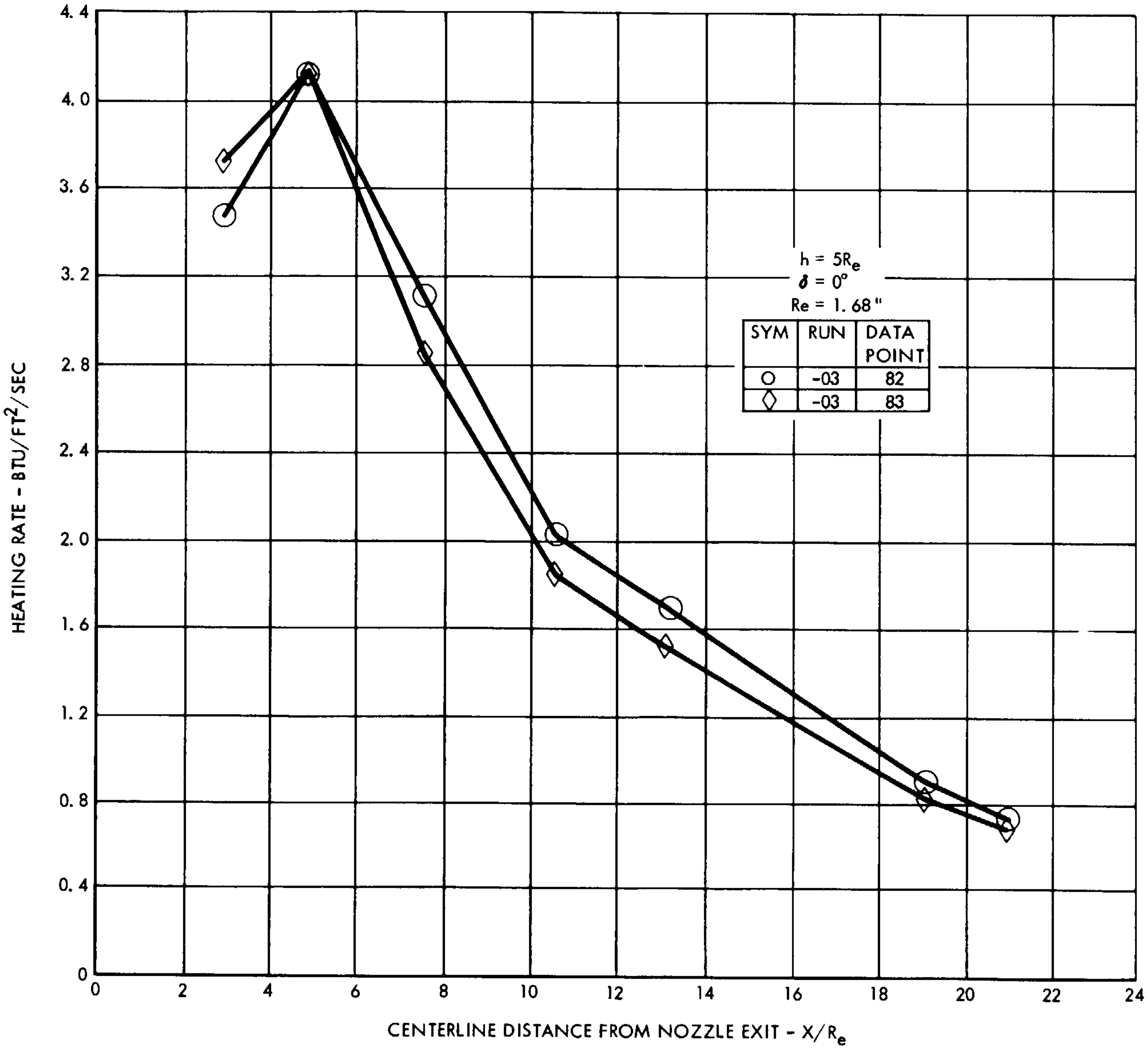

Figure 26. Heating Rate Distribution $\epsilon = 15:1$

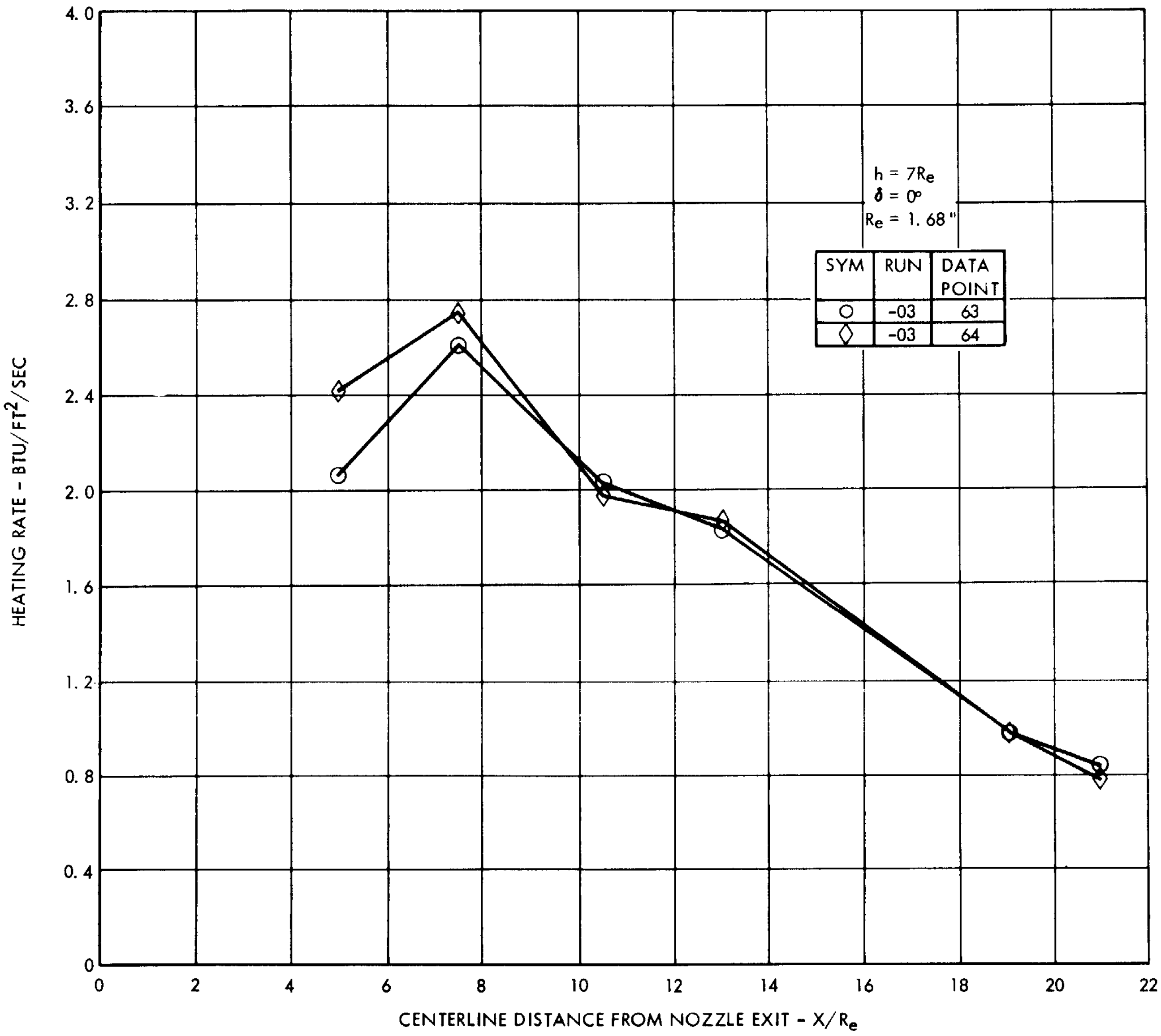

Figure 27. Heating Rate Distribution $\epsilon = 15:1$

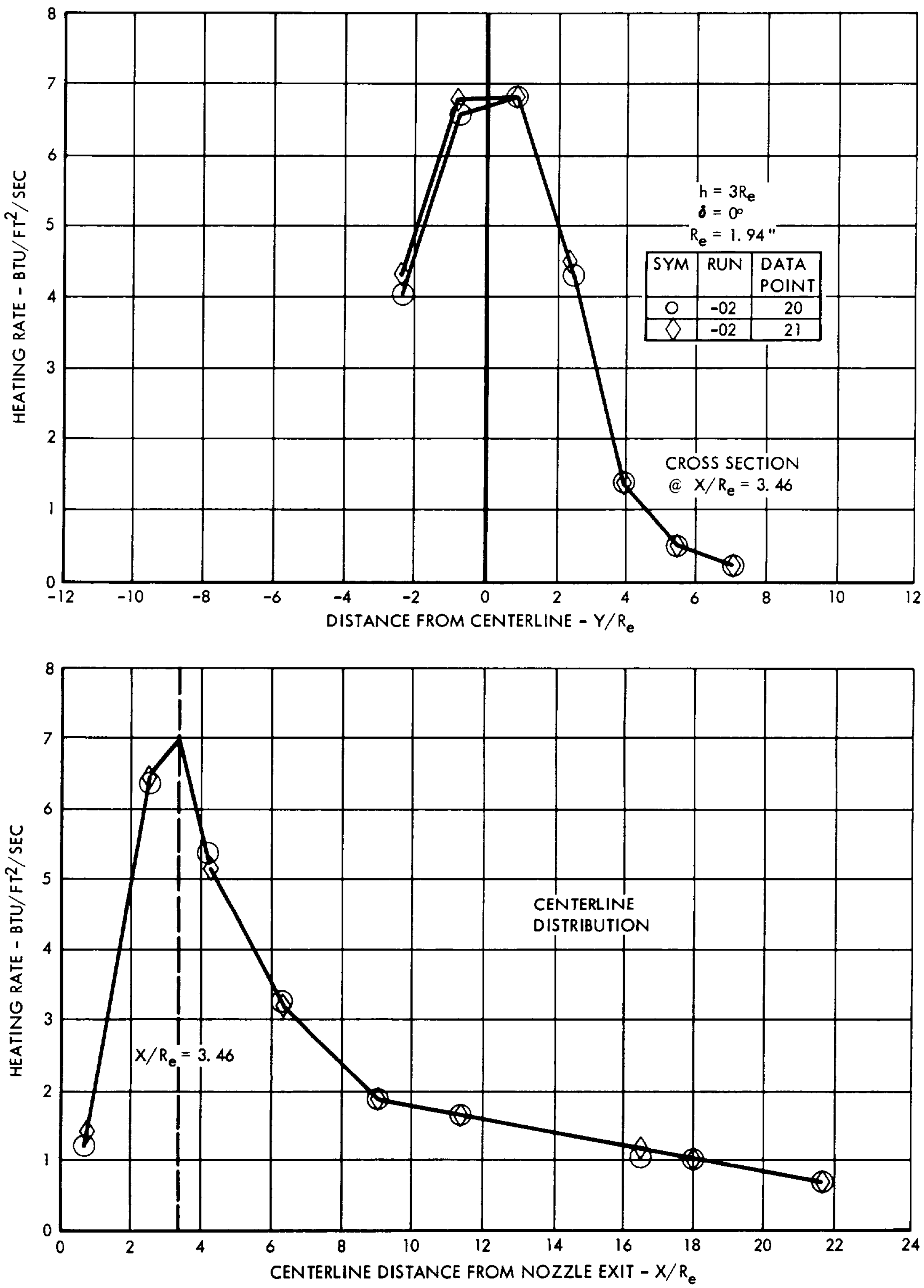

Figure 28. Heating Rate Distribution ϵ = 20:1

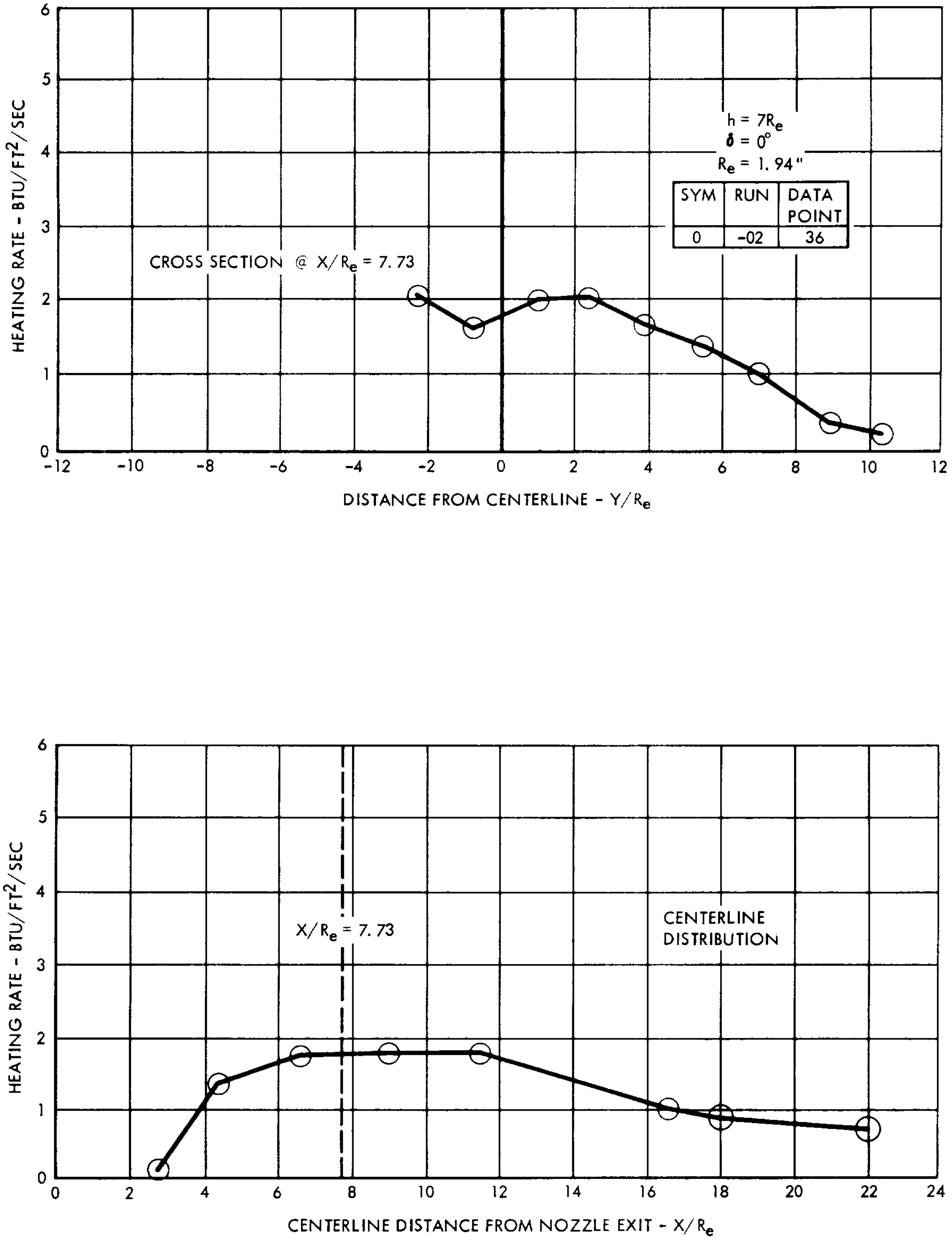

Figure 29. Heating Rate Distribution ϵ = 20:1

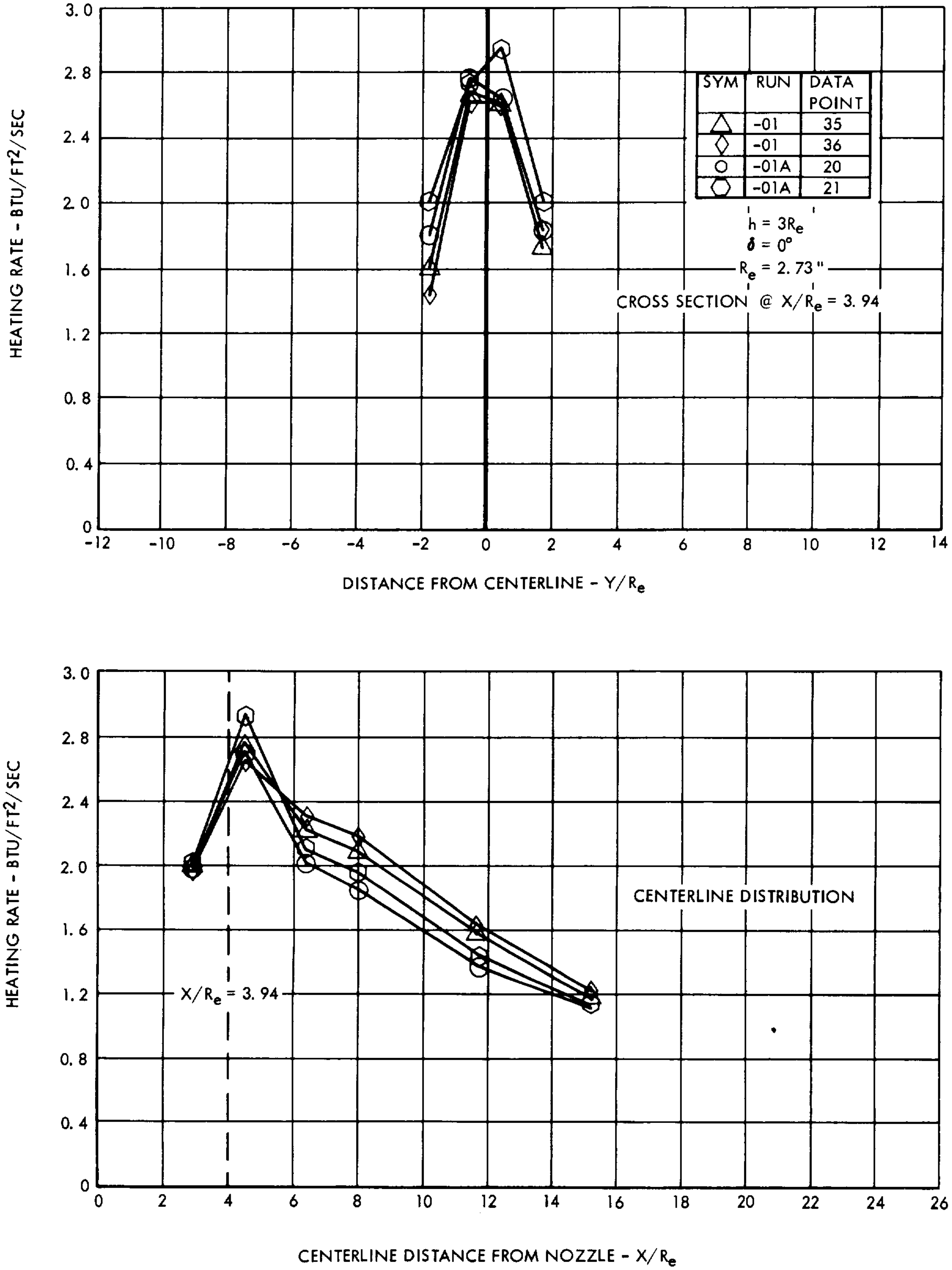

Figure 30. Heating Rate Distribution, ϵ = 40:1

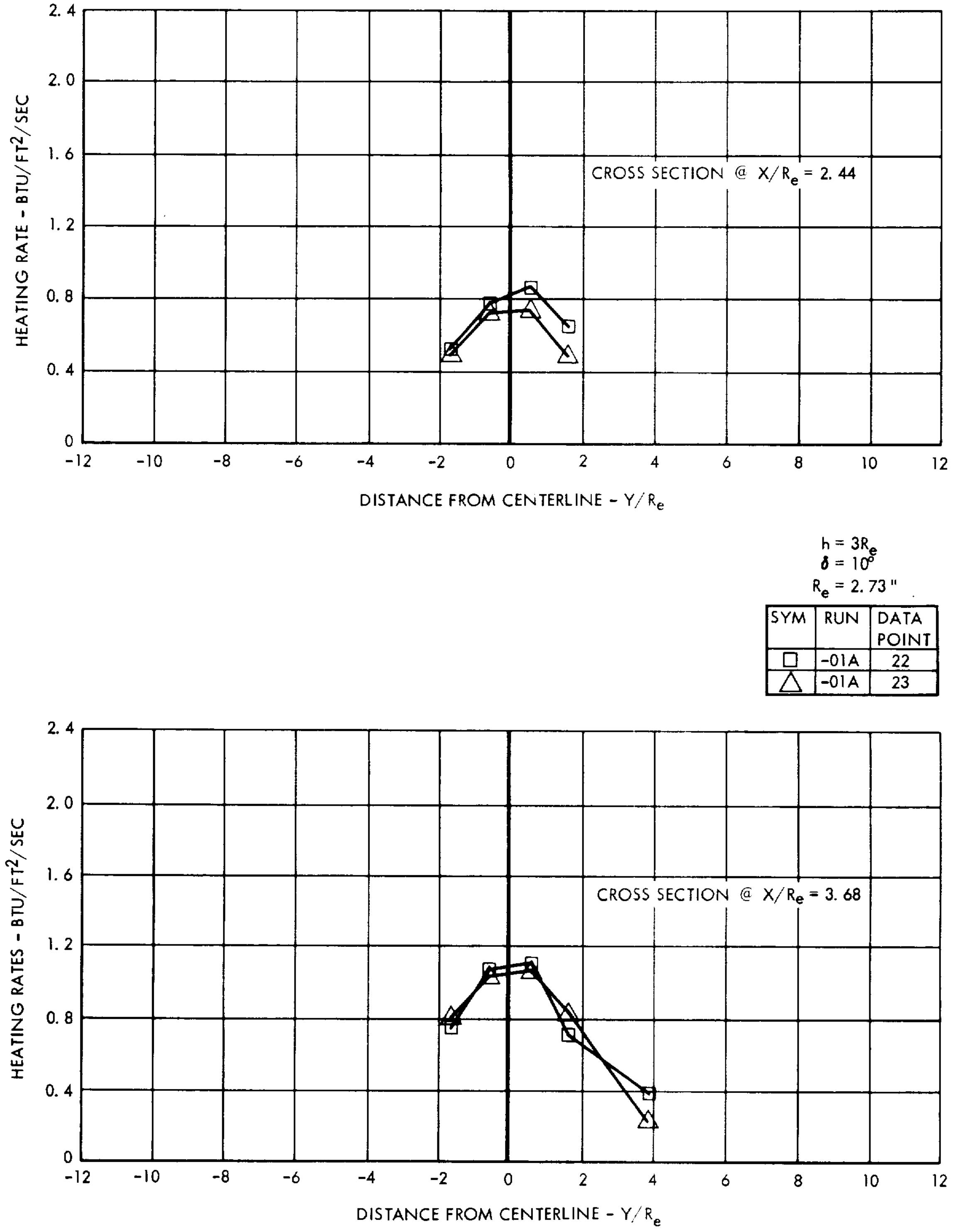

Figure 31. Heating Rate Distribution, Apollo SM RCS Design Case, ϵ = 40:1

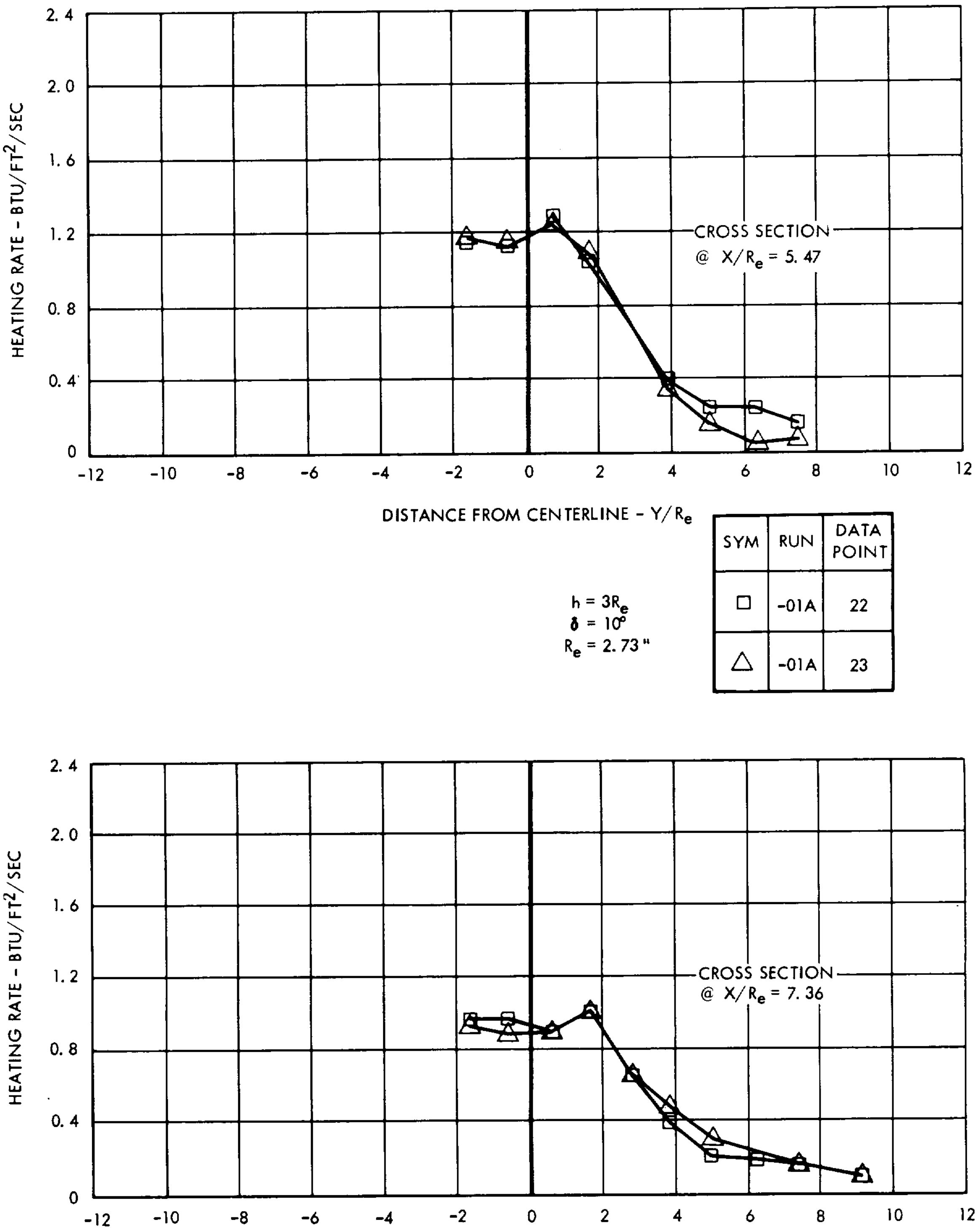

Figure 32. Heating Rate Distribution, Apollo SM RCS Design Case, ϵ = 40:1

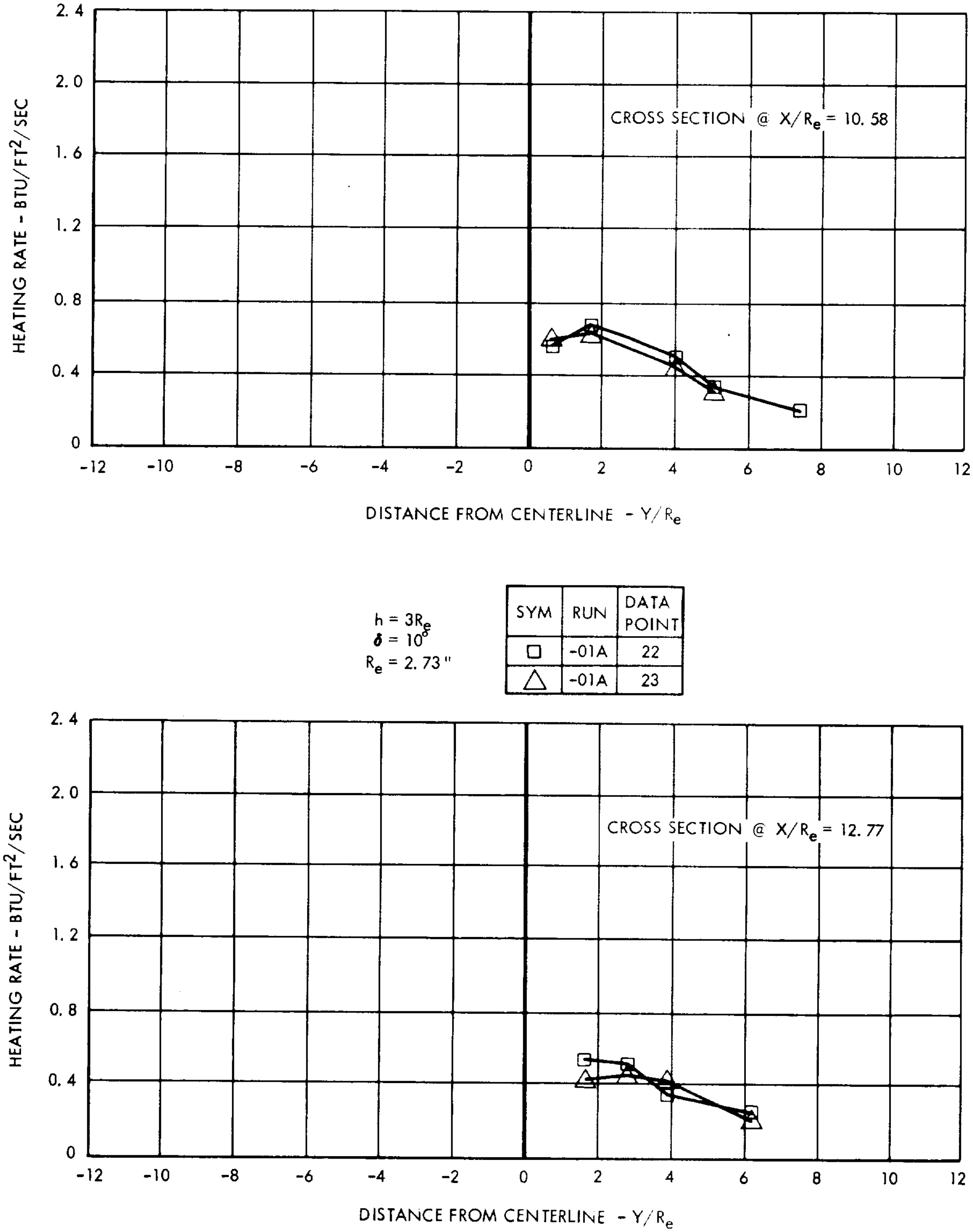

Figure 33. Heating Rate Distribution,
Apollo SM RCS Design Case, ϵ = 40:1

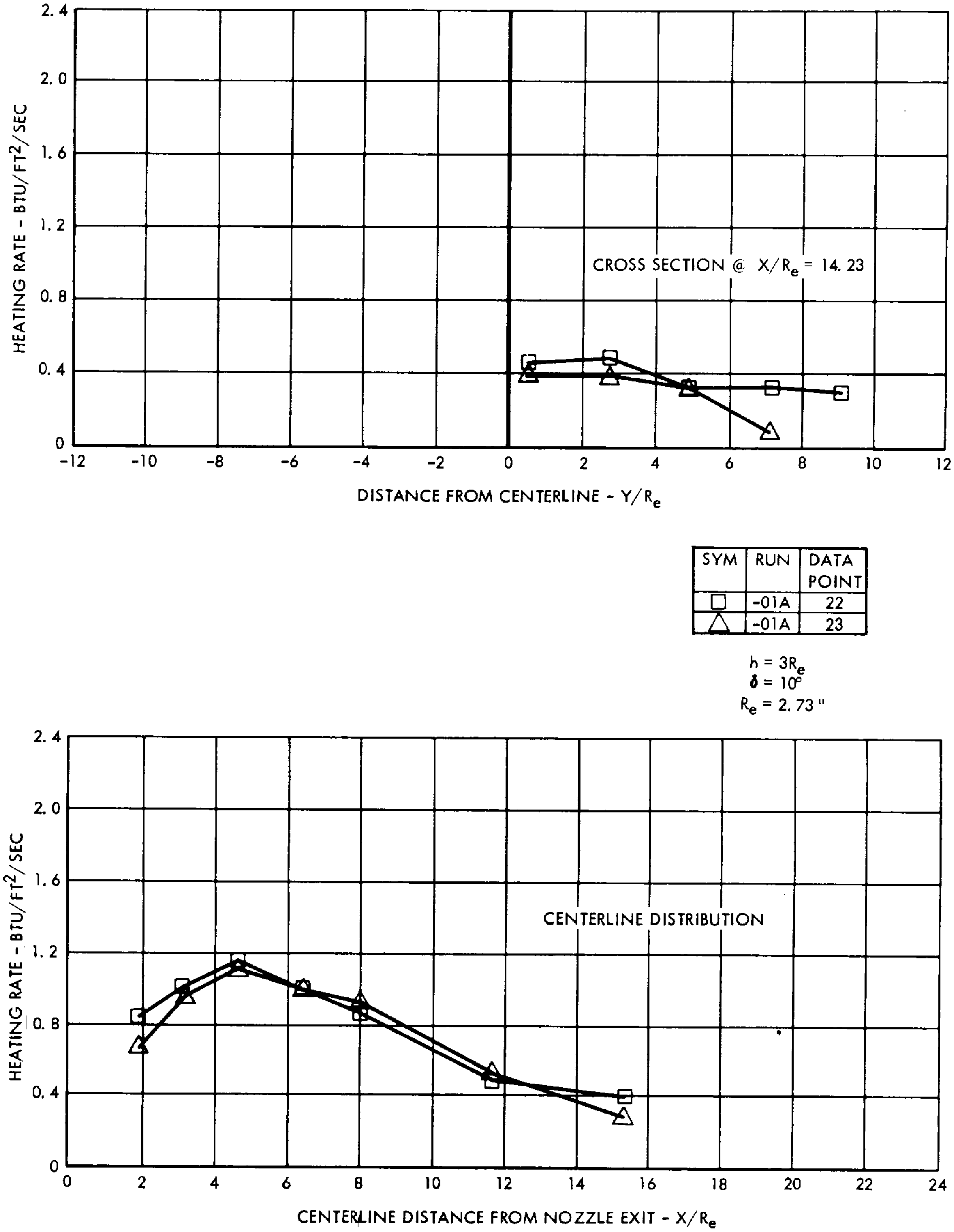

Figure 34. Heating Rate Distribution, Apollo SM RCS Design Case, ϵ = 40:1

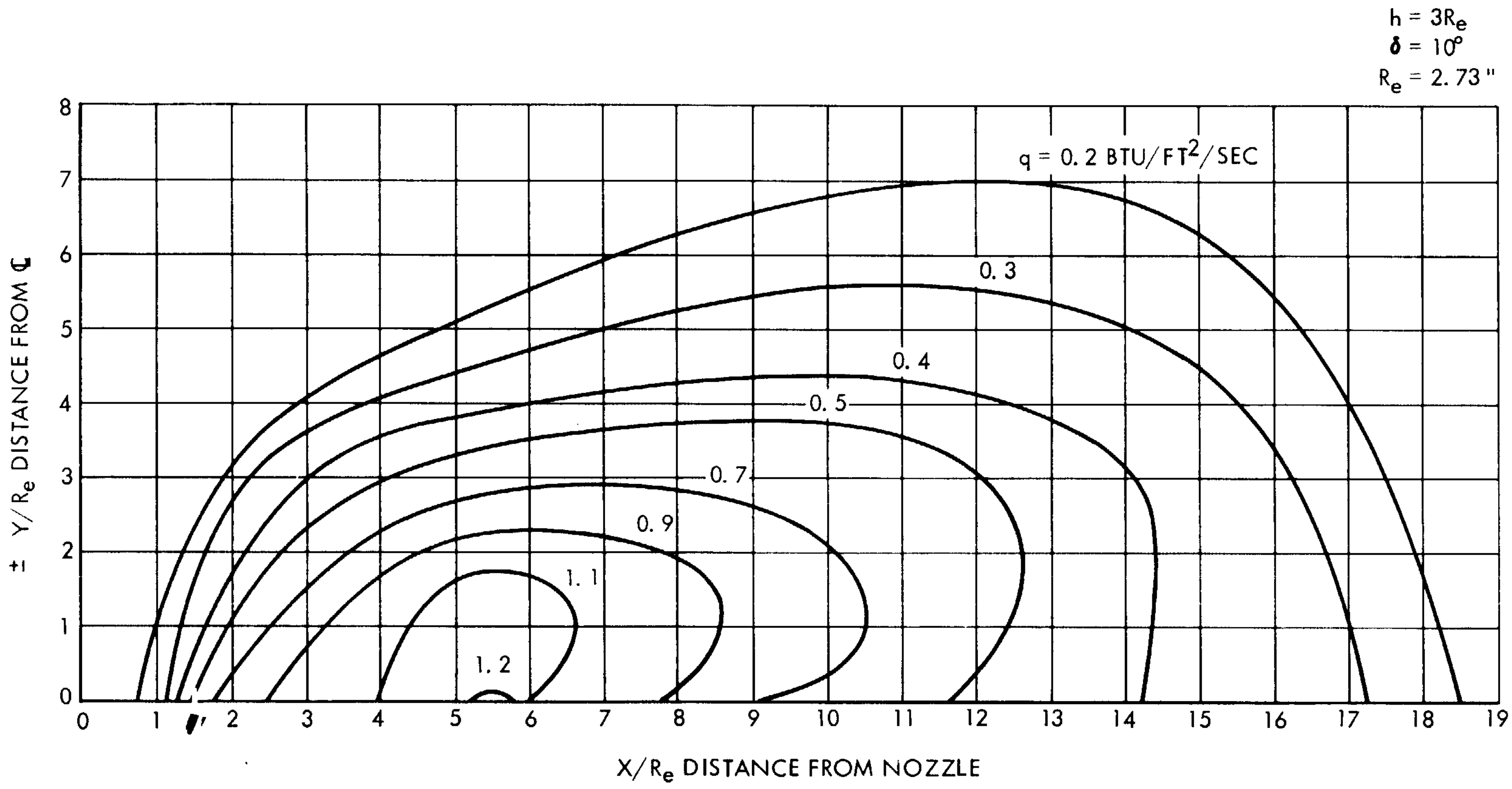

Figure 35. Heating Rate Map, Apollo SM RCS Design
Case ϵ = 40.1

line (0.2 BTU/ft^2/sec) is farthest from the centerline, the flat plate to SM surface deviation is less than three inches.

From the data for one particular nozzle area ratio and zero degree cant angle, but at various elevations, it is seen that the peak heating rate value decreases and its location moves downstream as the elevation-plate-to-nozzle centerline increases. Note that the centerline heating rate curves for the various elevations are coincident downstream of the peak value.

The highest surface pressures were obtained from the 10:1 area ratio nozzle placed three nozzle exit radii from the plate at zero-degree cant angle. These pressure data are presented in Figures 36 through 38.

The centerline heating rates and surface pressure distributions are compared in Figure 39 for the 10:1 area ratio, 3Re elevation and zero-degree cant angle. It is seen that the shape and the location of the peak values compare very favorably.

An attempt was made to obtain flow visualization of the rocket engine exhaust at conditions approaching those in space. The fuel, Aerozine 50, was saturated with sodium acetate to increase the luminescence of the exhaust. In an attempt to obtain a further increase in the visibility of the exhaust, a high voltage (11Kv) probe was placed inside the plume boundary to ionize the exhaust gases. A typical result of these attempts is shown in Figure 40. Additional flow visualization results and methods for empirically determining the plume boundary from the data of this test are given in reference 5.

During the 15:1 area ratio runs, a camera was located downstream of the nozzle, facing the nozzle exit, to determine the glare from the exhaust. Figure 41 shows the results from this camera and also a side view of the exhaust flow field. Note that the fuel was not seeded with sodium acetate on this run and the high voltage probe was not activated.

If one compares side views of the exhaust flow field (Figures 40 and 41) it can be seen that only with the sodium seeding does a significant portion of the flow field become visible. But head on, the exhaust glare appears significant even without propellant additives.

The test results pertaining to the effect of the exhaust on the life and surface properties of the radiator surface sample are not conclusive for the Apollo design. The results, however, do indicate that the surface properties were little affected by exhaust impingement during the one run (-01, $\epsilon = 40:1$) in which usable data was obtained. The total rocket engine firing time during this run was approximately 21 seconds.

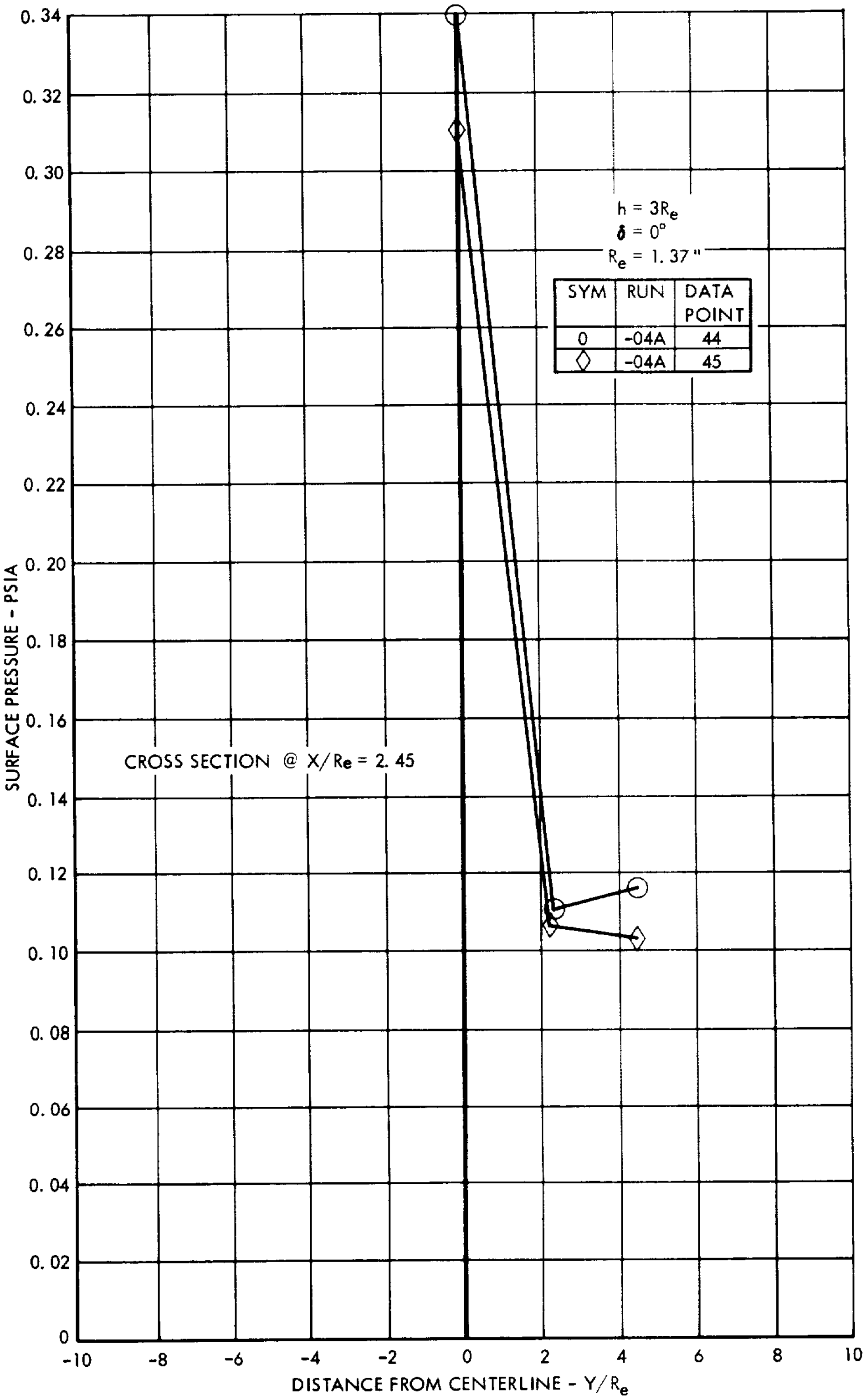

Figure 36. Surface Pressure Distribution, ϵ = 10:1

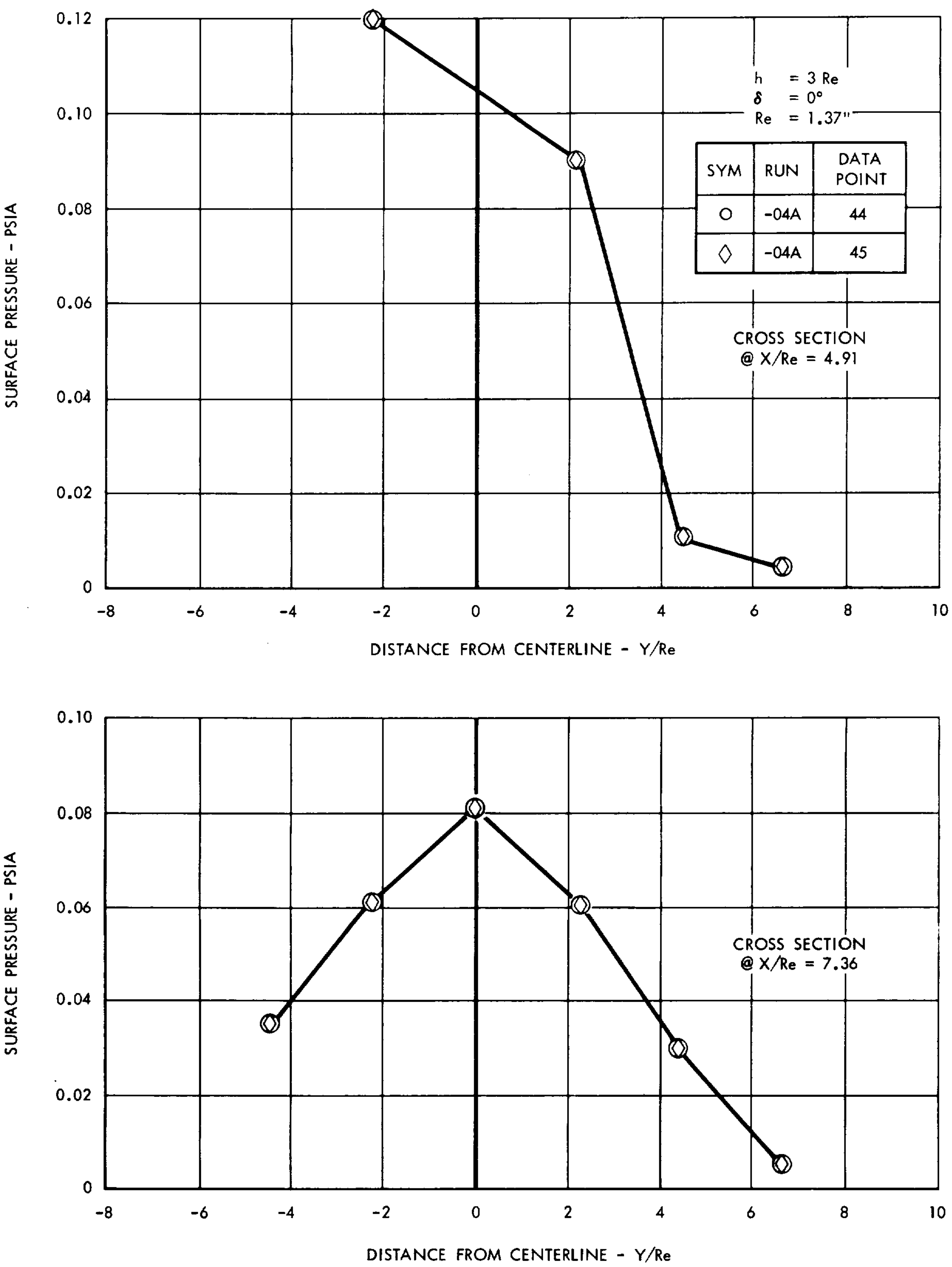

Figure 37. Surface Pressure Distribution, ϵ = 10:1

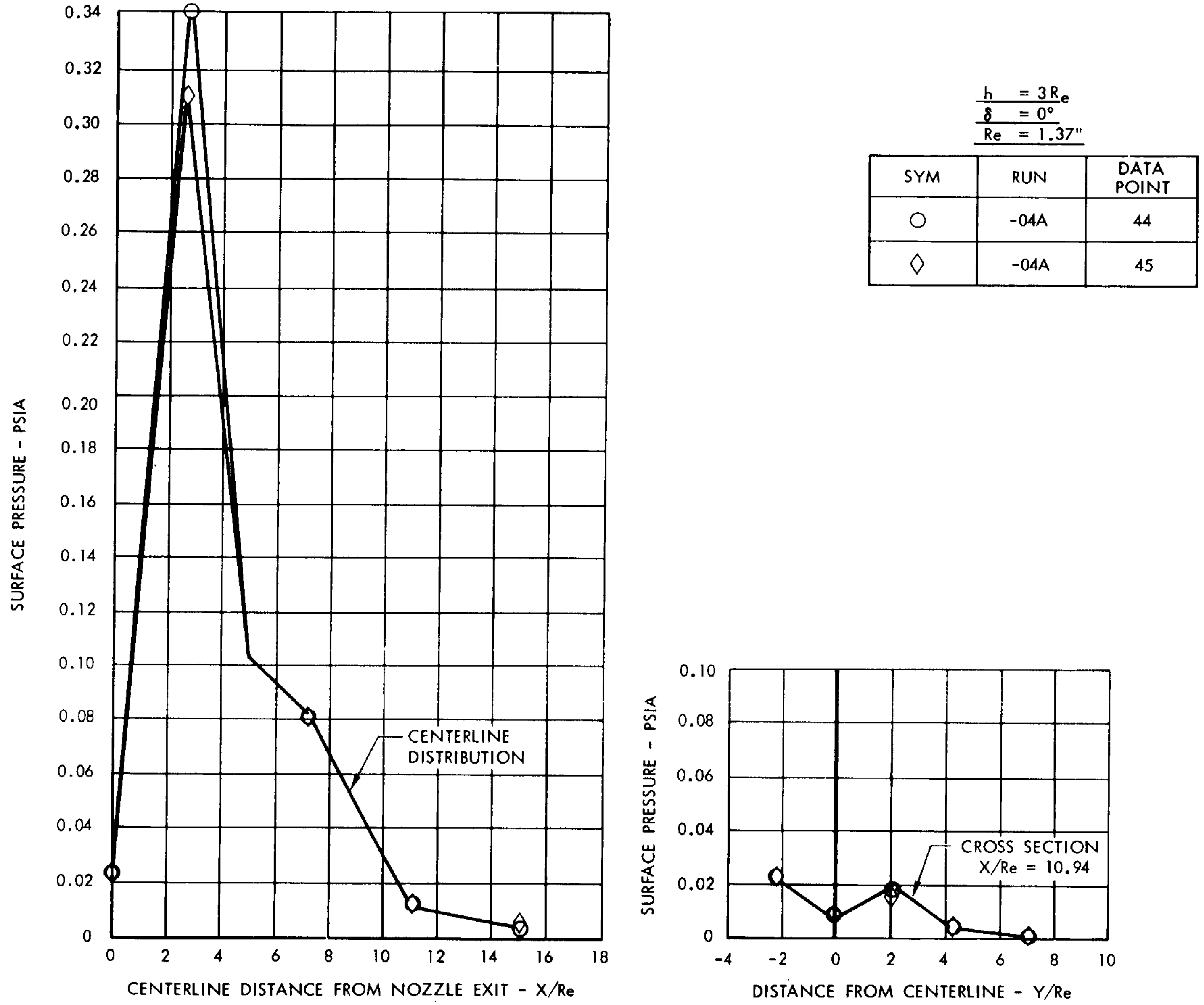

Figure 38. Surface Pressure Distribution, ϵ = 10:1

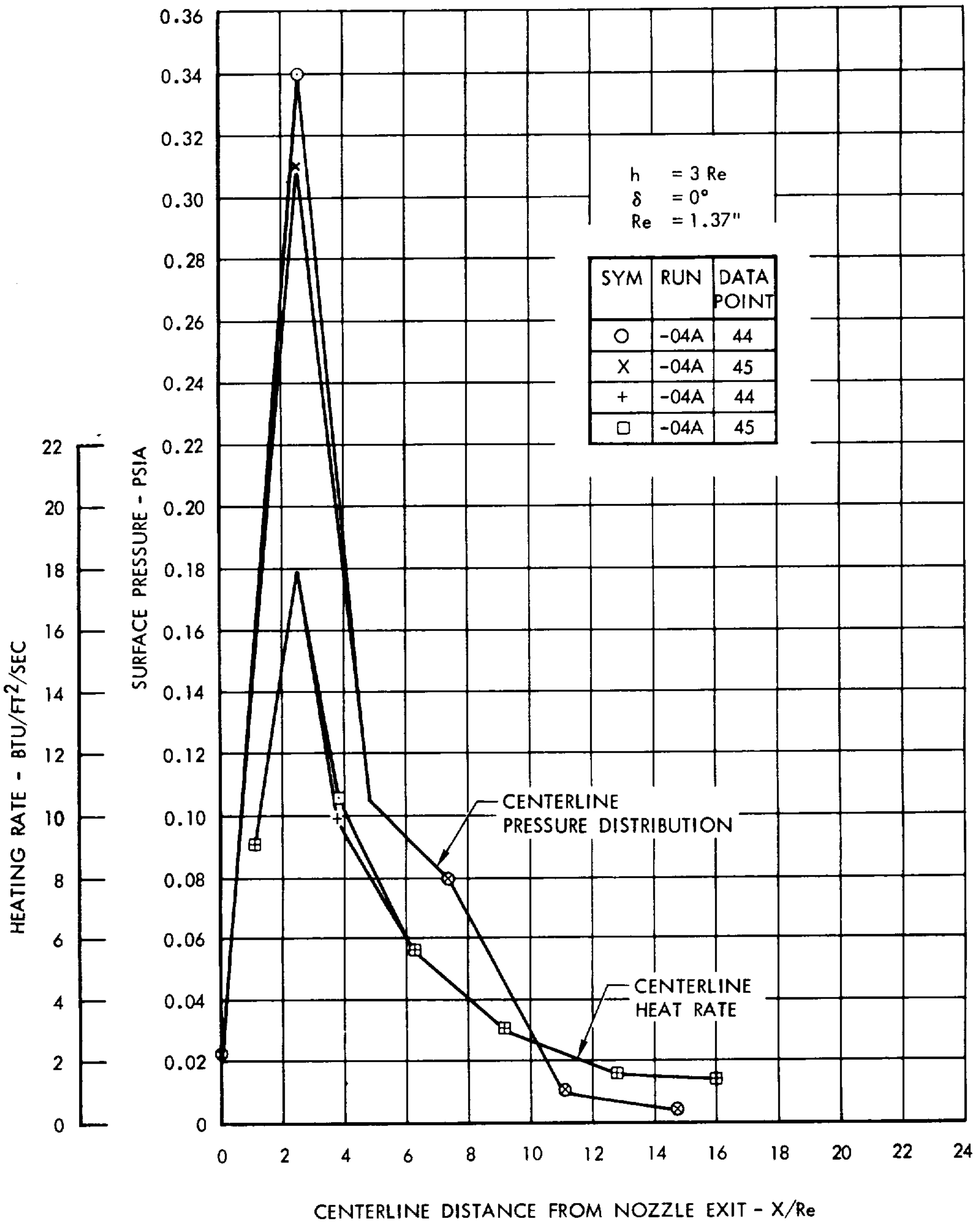

Figure 39. Comparison of Centerline Heating Rate and Pressure Distributions, ϵ = 10:1

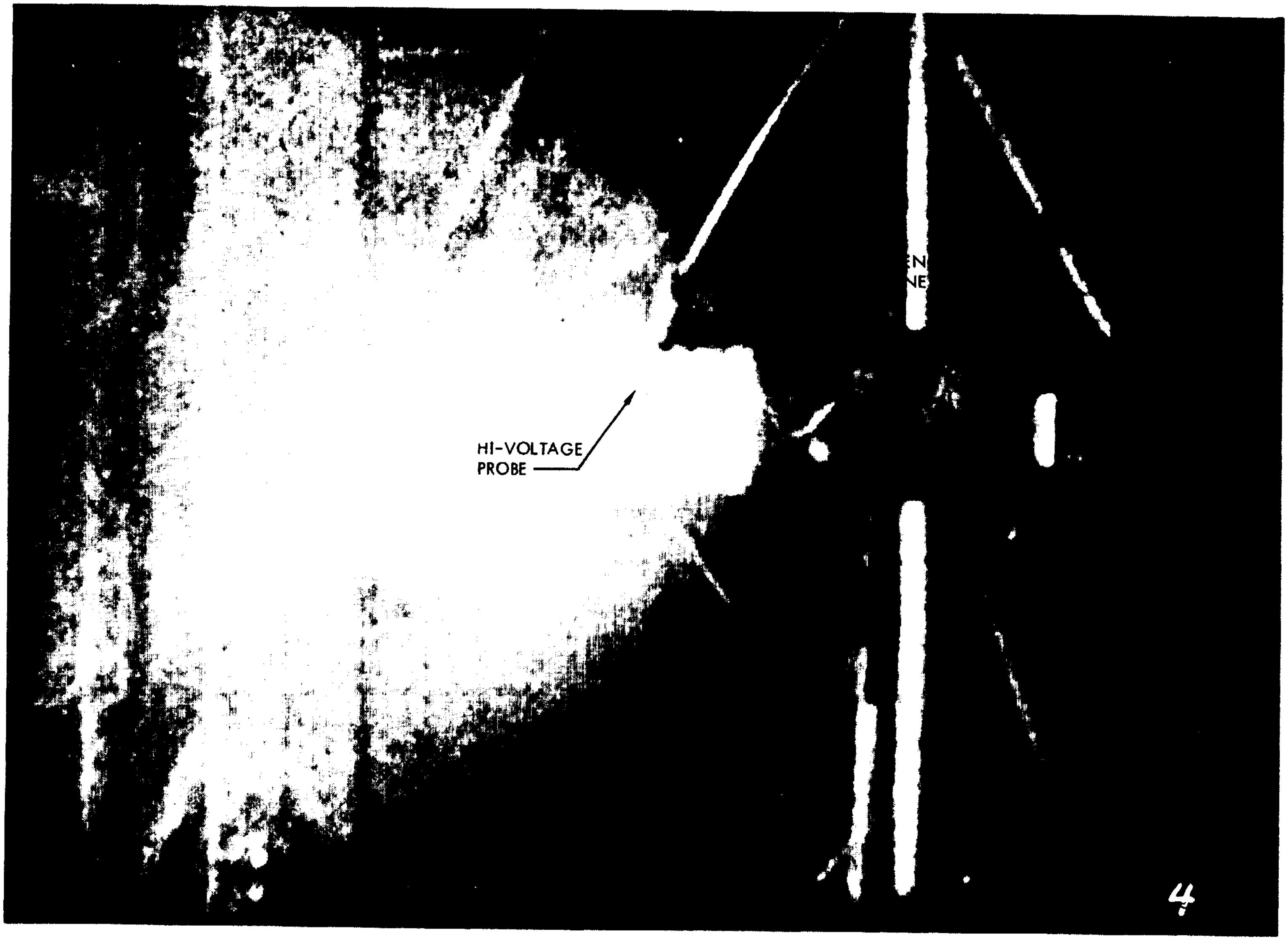
HI-VOLTAGE PROBE
4

Figure 40. Exhaust Flow Field Visualization $\epsilon = 40:1$

APOLLO SM/RCS NOZZLE EXHAUST

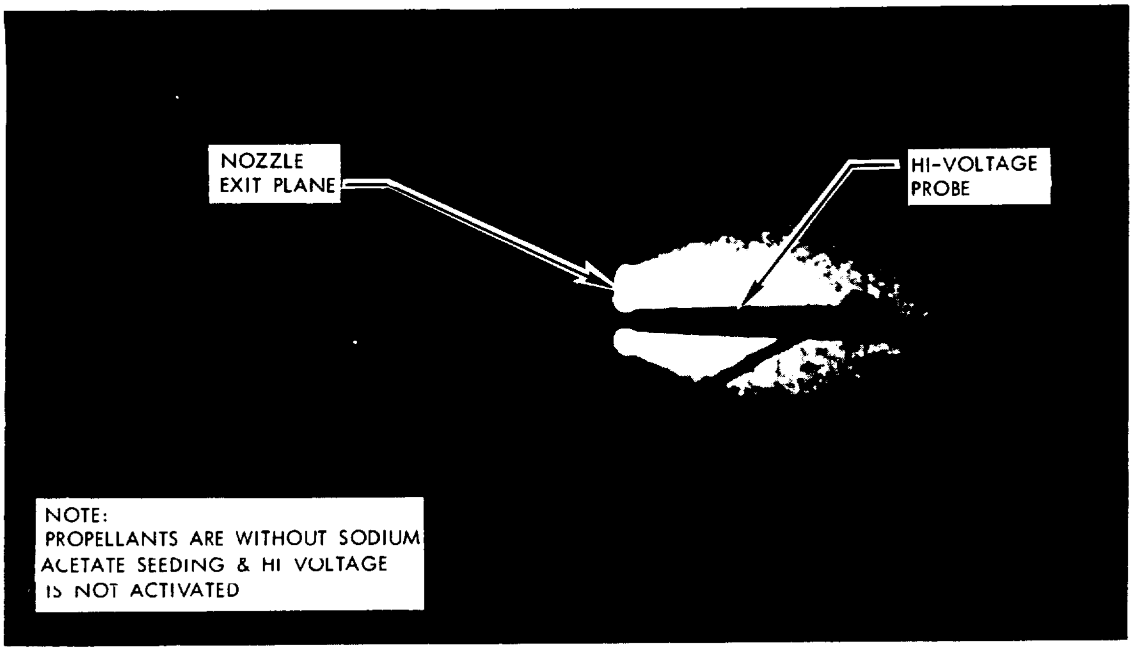
NOZZLE
EXIT PLANE
HI-VOLTAGE
PROBE
NOTE:
PROPELLANTS ARE WITHOUT SODIUM
ACETATE SEEDING & HI VOLTAGE
IS NOT ACTIVATED

SIDE VIEW NOZZLE EXHAUST
$\epsilon = 15$, $h = 12.8$ Re, $\delta = 25°$ $P_c/P_\infty \approx 1 \times 10^6$
RUN 03 DATA POINT 23 8 FRAMES/SEC

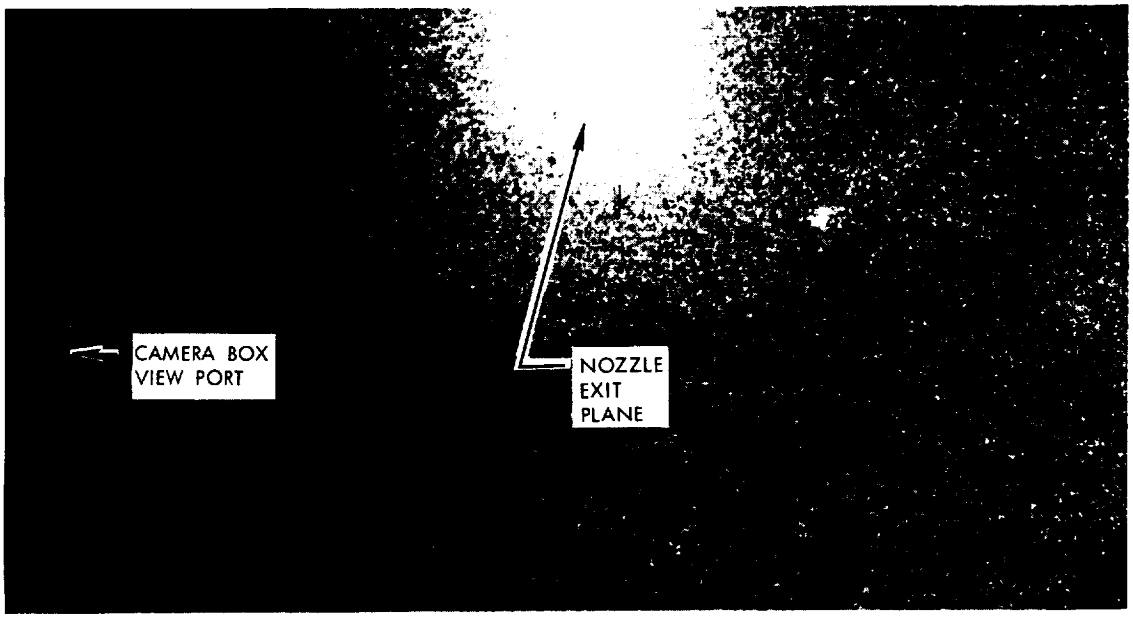
CAMERA BOX
VIEW PORT
NOZZLE
EXIT
PLANE

FRONT VIEW - NOZZLE EXHAUST
$\epsilon = 15$, $h = 12.8$, $\delta = 25°$, $P_c/P_\infty \approx 1 \times 10^6$
RUN 03 DATA POINT 23 8 FRAMES/SEC

Figure 41. Exhaust Flow Field Visualization $\epsilon = 15:1$

V. CONCLUSIONS

From the data presented in this report several significant conclusions can be drawn concerning the characteristics of a high-altitude exhaust flow field and its effect on a nearby structure.

1. The design of a light weight stainless steel heat shield to protect the Apollo SM surface from the SM RCS exhaust impingement has been shown to be feasible by the heating rates experimentally defined in this test.
2. The experimental data presented verifies that the surface properties due to any particular exhaust flow field impingement configuration on a flat plate do not vary with ambient pressure (over the range tested) inside the region of the plume boundary shock.
3. For a particular nozzle, the centerline heating rate peak decreases and moves downstream as the plate elevation increases; the heating rate values downstream of the peak are coincident for the range of elevations tested at zero-degree cant angle.